We are IntechOpen,
the world's leading publisher of
Open Access books
Built by scientists, for scientists

6,900
Open access books available

185,000
International authors and editors

200M
Downloads

154
Countries delivered to

Our authors are among the

TOP 1%
most cited scientists

12.2%
Contributors from top 500 universities

CLARIVATE ANALYTICS
BOOK CITATION INDEX
INDEXED

WEB OF SCIENCE™

Selection of our books indexed in the Book Citation Index
in Web of Science™ Core Collection (BKCI)

Interested in publishing with us?
Contact book.department@intechopen.com

Numbers displayed above are based on latest data collected.
For more information visit www.intechopen.com

Holographic Image Storage with a 3-Indoly-Benzylfulgimide/PMMA Film

Neimule Menke[1] and Baoli Yao[2]
[1]School of Physical Science and Technology,
Inner Mongolia Universtiy
[2]State Key Laboratory of Transient Optics and Photonics,
Xi'an Institute of Optics and Precision Mechanics, Chinese Academy of Sciences
China

1. Introduction

Fulgide is well-known as a thermally irreversible organic photochromic compound [1,2]. It is one of the important materials in the field of optical signal processing and optical storage. Focusing on the holographic storage applications of 3- indoly-benzylfulgimide/PMMA film, in this chapter include the following themes.

In section 2, first the Fulgide, photochroism and photo-induced anisotropy are introduced. Then the spectra and kinetics of the photochromic and photo-induced anisotropic properties of 3-indoly-benzylfulgimide/PMMA film were studied.

In section 3, the applications of ordinary holography and polarization holography of fulgide film were studied, which were respectively based on the photochromic and photo-induced anisotropy properties. The properties of holographic recording such as diffraction efficiency, spatial resolution and optimal exposure were measured.

In section 4, the holographic optical image storage was realized in a 3-indoly-benzylfulgimide/PMMA film by using different kinds of holographic storage techniques, e.g., transmission-type holographic recording and reflection-type holographic recording, reference beam reconstruction and phase conjugated beam reconstruction, Fraunhofer holographic recording and Fourier-transform holographic recording, different kinds of polarization holographic recording (i.e. parallel linear polarization holographic recording, orthogonal linear polarization holographic recording, parallel circular polarization holographic recording and orthogonal circular polarization holographic recording etc.), and collinear holographic storage technology etc. The diffraction efficiencies and diffractive images' signal-to-noise-ratios (SNR) of different kinds of holograms were compared. The storage density of 2×10^8 bits/cm^2 was obtained in the Fourier-transform holographic data storage by using orthogonal polarization holographic recording, which had a greatly improved signal-to-noise ratio of the diffraction image. And different kinds of multiplexing holographic storage (like polarization multiplexing, circumrotation multiplexing and angle multiplexing) and holographic interferometer were realized in the film.

2. Definition of fulgide, photochroism and photo-induced anisotropy

2.1 Photochroism

"Photochromism"is simply defined as a light-induced reversible change of color. "Photochromism is a reversible transformation of a chemical species induced in one or both directions by absorption of electromagnetic radiation between two forms, A and B, having different absorption spectra".The thermodynamically stable form A is transformed by irradiation into form B. The back reaction can occur thermally or photochemically (like shown in Fig.1) [2,3].

$$A \overset{hv_1}{\underset{hv_2\ /\triangle}{\rightleftharpoons}} B$$
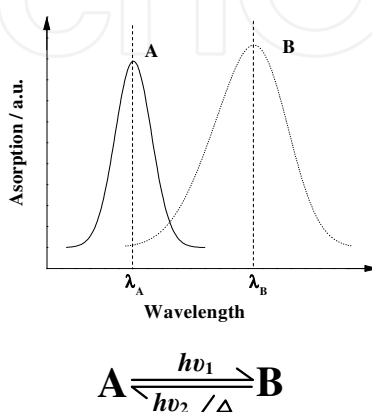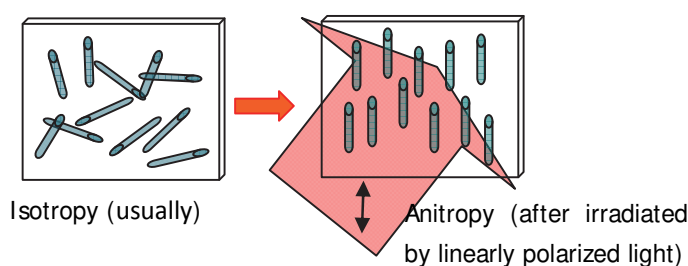
Fig. 1. A simple sketch map of photochromic

Fig. 2. A simple sketch map of the mechanism of photo-induced anisotropy

2.2 Photo-induced anisotropy

In transparent materials with anisotropic dielectric permittivity, optical anisotropy can be observed, in which include the pleochroism (anisotropy of the material's absorption coefficient) and birefringence (anisotropy of the material's refractive index). **Pleochroism** means that the absorption of the material to the light depends not only on the wavelength of light, but also on the polarization state of light: for uniaxial crystals, it is called as **dichroism**; for biaxial crystals, it is called as **trichroism**. **Birefringence** means that the refractive index of the material depends not only on the wavelength of light, but also on the polarization state of light.

Many crystals have crystal lattice structure themselves, so they are **natural optical anisotropic media**. However, in some amorphous material, under the action of certain external field (such as electromagnetic fields, mechanical forces, etc.), their atoms or molecules will be orientated in certain rules, thus the material will change from isotropic into anisotropic macroscopically, which is called as the **artificial optical anisotropy**. In

which, under the irradiation of polarized light, some isotropic materials will turn to be anisotropic, or the degree of anisotropic properties in some materials will change, this phenomenon is called as the **photo-induced anisotropy** (like shown in Fig.2). Which include the photo-induced dichroism (usually photo-induced anisotropic materials show the properties of uniaxial crystal) and photo-induced birefringence.

2.3 Fulgide
2.3.1 Structures of fulgides
Early in 20th century, Stobbe and Eckert, (Leipzig University, Germany) [1,2] found that the condensation products of succinate and aromatic group of aldehydes, ketones have photochromic property. They stated in their article in 1905 that they named the derivatives of 1,3-butadiene-2,3-dicarboxylic acid and its acid anhydride as "fulgenic acid " and "fulgide", respectively (like shown in Fig.3), after the Latin word "fulgere" (glitter or shine), because some derivatives exhibited a variety of characteristic colors by light, and they usually formed shiny crystals.
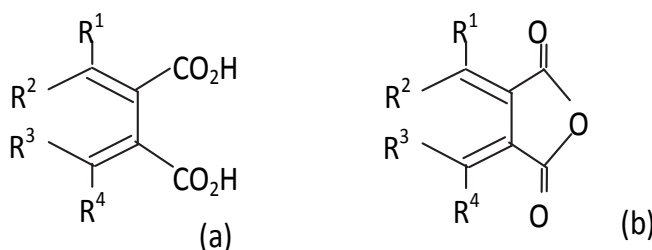
Fig. 3. Chemical molecular formula of the fulgenic acid (a) and fulgide (b)

To be photochromic, fulgides should have at least one aromatic ring or heteroaromatic ring (Ar) on the exo-methylene carbon atom, so that they form a 1,3,5-hexatriene structure that may undergo 6π-electrocyclization.

When three of the four substituents are same, the fulgide compounds have two isomers: cis-isomer and trans-isomer. According to geometrical shape of the double bond connecting the aromatic ring and succinic acid, they are called as "E-form" And "Z-form" respectively (for example, the isomers of phenyl fulgide are shown in Fig.4). In which, the E-form has an "all cis-hexatriene" structural unit, so it can be photocyclized. When two of the four substituents are same, the fulgide compounds have three isomers: (E,E), (E,Z) and (Z,Z). When the four substituents are different with each other, the fulgide compounds have four isomers: (E,E), (E,Z), (Z,E) and (Z,Z).
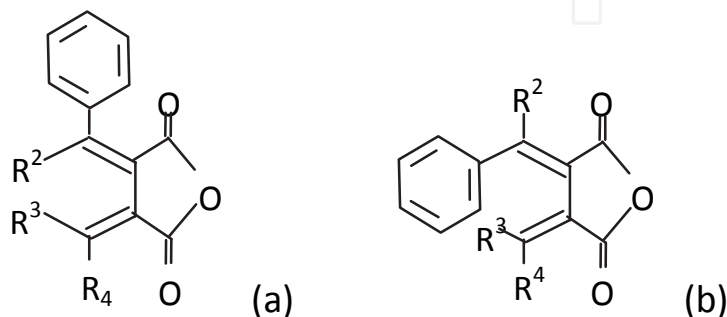
Fig. 4. The two isomers of phenyl-fulgide: (a) Z-form; (b) E-form

2.3.2 The photochroism of fulgides

The photochroism of fulgide occurs between one of the colorless open forms "E-form" and the photocyclized colored form (abbreviated as the C-form), like shown in Fig.5. The coloration mechanism of fulgide is the photochemical 6π-electrocyclization of the hexatriene moiety, is a cyclic reaction consistent with Woodward-Hoffmann selection rules. However, there exits an additional photochemical E-to-Z isomerization, the Z-form is not considered as an important component in the photochromic system. There has been no report that the Z-form cyclizes directly by absorbing on photon to give the C-form. Therefore, E-to-Z isomerization, competing with the photochromic E-to-C isomerization, is an energy-wasting as well as system-complicating process in terms of the "photochroism of fulgides". Using Improvement of the structure, this additional reaction can be suppressed. Usually E- and Z-forms have maximum absorption in the UV region; C-form has maximum absorption in the visible region .
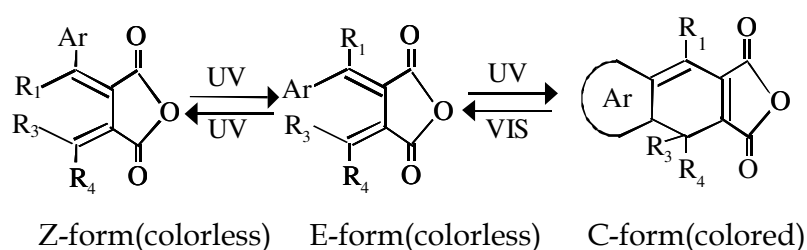

Z-form(colorless)   E-form(colorless)   C-form(colored)

Fig. 5. The photochromic reaction of fulgides

2.3.3 The derivatives of fulgide

The photochromic mechanism of fulgide is the photochemical 6π-electrocyclization process, so the carbonyl group and the aromatic ring are both not indispensable. For example, anhydride part can be instead of other functional groups, like succinimides (fulgimide), butanolides (fulgenolide), dieters (fulgenate) and compounds having an anhydride ring with modified carbonyl group (as shown in Fig.6) [1,2].
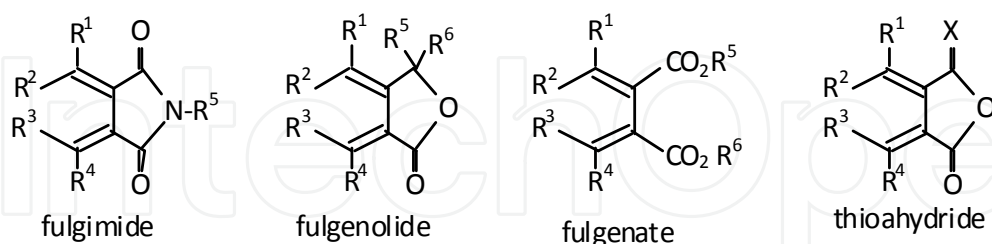

fulgimide   fulgenolide   fulgenate   thioahydride

Fig. 6. Chemical molecular formula of the fulgide derivatives

2.3.4 The photo-induced anisotropy of fulgide films

We found that there exists photo-induced anisotropy in fulgide-doped polymeric films [4], which can be used in polarization holography application. When the colored states are irradiated by a linearly polarized 650 nm laser, the films returns to the bleached states and photo-induced anisotropy is produced during this process. The mechanism of photo-induced anisotropy in the fulgide films is the following [4]: anisotropic absorbing molecules of fulgide are immobilized randomly in the PMMA polymeric matrix, which shows

isotropic characteristic at the initial state; when the sample is irradiated by linearly polarized light photo-selection of molecules take place. Molecules with long axes parallel to the exiting light polarization direction absorb the light strongly and turn to the other form very quickly, whereas those with long axes perpendicularly orientated to exiting light polarization have low absorption and stay at the initial form. As a result special orientation of two form molecules is induced and the sample shows optical anisotropy properties macroscopically. The angular distributions of molecules in anisotropy inducing progress are shown in Fig.7. So, under the irradiation of circularly polarized light, the sample shows also optical isotropy.
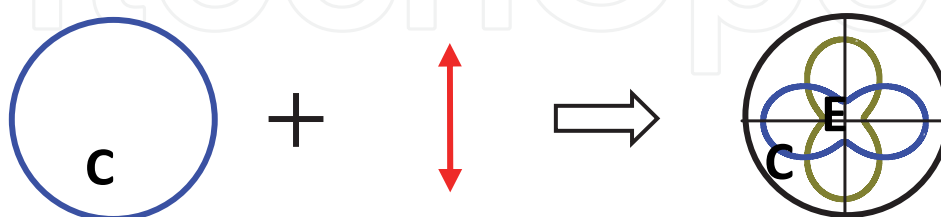
Fig. 7. Angular distributions of molecules in anisotropy inducing progress

2.4 Holographic storage application of fulgide films

Photochromic organic compounds show great potential in the field of rewriteable holographic storage owing to its benefits like lower price, higher signal noise ratio (SNR), higher spatial resolution, higher sensitivity, less toxic, no need to special fixing information after recording, stable in the air or moisture, and easy to be modulated [1,2]. Their disadvantages are lower diffraction efficiency and difficulty to realize non-destructive readout. In which, fulgides are famous as thermally irreversible organic photochromic compounds.

The photochromic and photo-induced anisotropic properties of materials can be used in ordinary and polarization holographic recording respectively. It is known that fulgide-doped polymeric films are photochromic and photo-induced anisotropic, which can be used for both.

For isotropy photochromic materials, only when the object light $\vec{O}$ and reference light $\vec{R}$ have components with same polarization state, there the intensity grating exists and the holograms can be recorded, called as **ordinary hologram**. But for photo-induced anisotropic materials, even if the $\vec{O}$ and $\vec{R}$ have orthogonal polarization states, the holograms also can be recorded, because that at this time although the intensity of the superposed light is a constant, but its polarization state changes with the phase difference between $\vec{O}$ and $\vec{R}$. Photo-induced anisotropic materials can record the polarization state of exciting beam, so the holographic gratings can be recorded, called as **polarization hologram**, in which not only the intensity and phase signals of $\vec{O}$ can be stored (the photo-induced anisotropy is depending on the exposure), but also its polarization state can be stored.

Here we just consider four kinds of polarization holographic storage, including the parallel linearly, parallel circularly, orthogonal linearly and orthogonal circularly polarized holograms. Fig.8 is a simple sketch map showing the space modulation of the distributions and orientations (optical axis) of C-form and E-form molecules of fulgide films in these four kinds of polarization holographic storage under the linearity recording condition when *O=R=A*. The arrows and ellipses on the horizontal line indicate the periodical distributions

of intensity magnitudes and polarization states of the recording field corresponding to the different phase differences $\Delta\varphi$ along the *x*-axis. The rectangle frames under them indicate the distribution and orientation of the molecules under the corresponding light irradiations, where the black and white color indicate the C-form and E-form molecules respectively, and the arrows indicate the direction of induced optical axes, and the star flower (✳) means the sample is isotropic at the place.
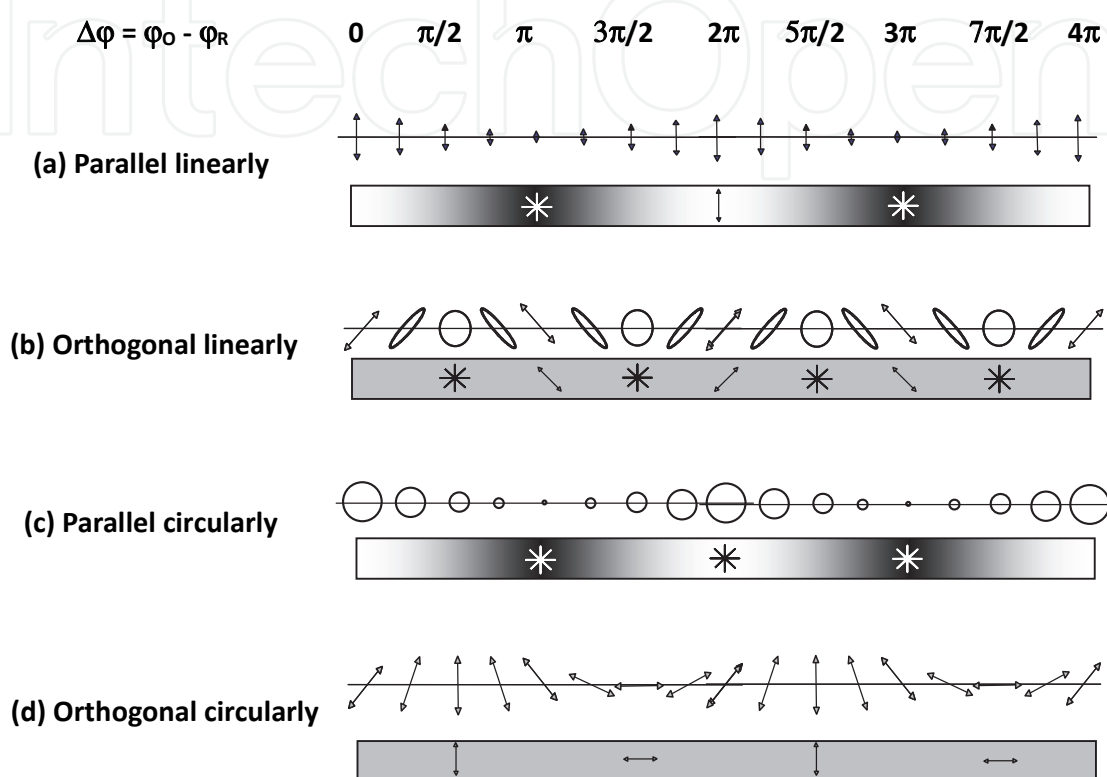

Fig. 8. The distributions of the interference fields in four kinds of polarization holography storage and the corresponding molecular distributions and orientations

From Fig.8, it can be seen that in the parallel circularly polarized hologram just ordinary hologram exits, and in the orthogonal polarized condition, just polarization hologram exits, but in the parallel linearly polarized holography, the ordinary hologram and polarization hologram will be recorded together.

2.5 Photochroism and photo-induced anisotropy of 3-indoly-benzylfulgimide/PMMA film

2.5.1 Material

The fulgide material studied here is 3-indoly-benzylfulgimide, which was synthesized by the Stobbe condensation routine [2]. The target compound of 3mg was dissolved in a 0.lml 10% (by weight) PMMA-cyclohexanone solution. Then the solution was coated on a 1-mm thick K_9 glass plane (Ø 25 mm × 1.5 mm) with a spin coater and dried in air. The thickness of the film is determined to be about 10μm by microscopy of the cross section. The photochromic or photo-induced anisotropic properties of fulgides are due to a reversible photochromic (photoisomerization) reaction that occurs between one of the colorless E-form (bleached state) and the C-form (colored state). These are the two spectrally separated

photochromic forms, whose molecular formulas are shown in Fig.9. In this film we also found the photo-induced anisotropy property [4].
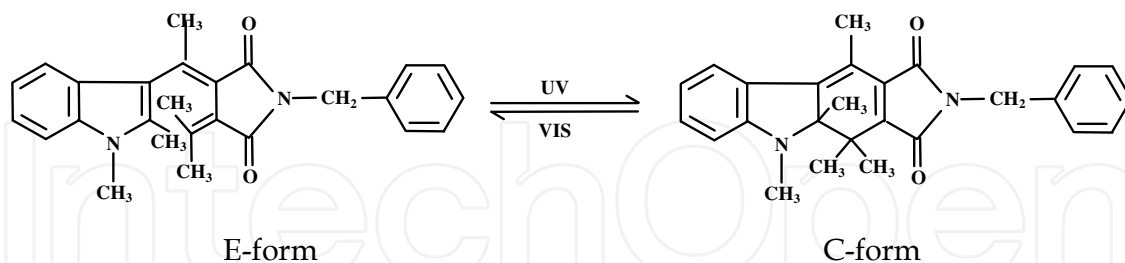

Fig. 9. Molecular formula of the Indolyfulgimide and the photochromic reaction. Left, E-form; right, C-form

2.5.2 Spectra of photochromic and photo-induced anisotropy properties of the sample

The absorption of the C-form ($A_C(\lambda)$) and E-form film ($A_E(\lambda)$) were measured using a UV-VIS-IR spectrophotometer (UV-3101PC, Shimadzu Inc., Japan), which were shown in Fig.10a. And the measurement of the photo-induced dichroism is performed by measuring the transmission spectra of the film for testing light polarized parallel ($T_{//}(\lambda)$) and perpendicular ($T_\perp(\lambda)$) to the polarization direction of the exciting beam after the C-form film is excited by the linearly polarized 650 nm laser (shown in Fig.11a).
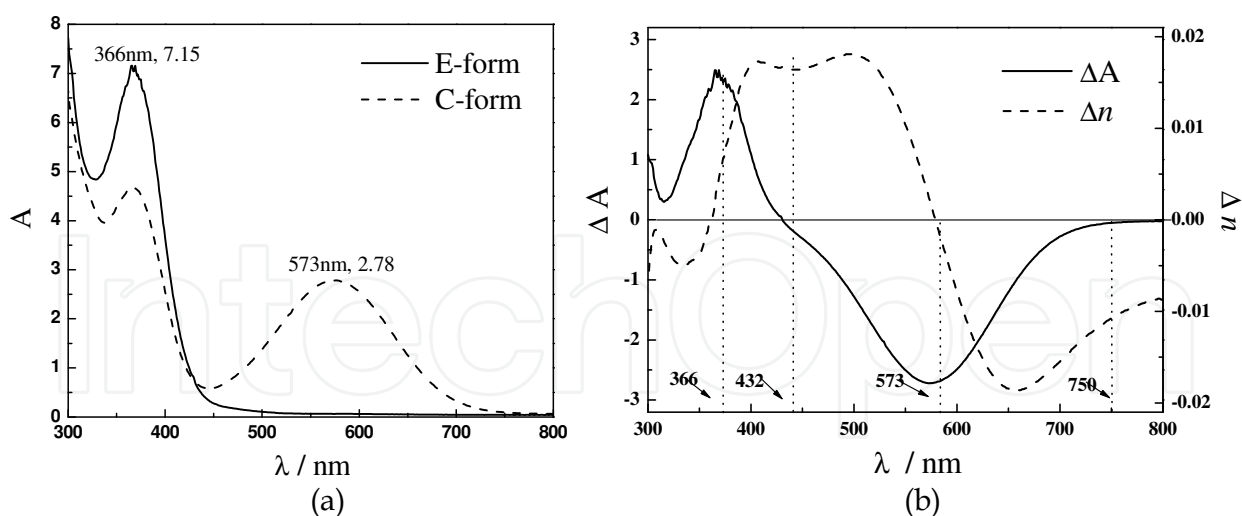
Fig. 10. Spectra of photochromic properties of Indolyfulgimide /PMMA film:(a) Absorption spectra of two forms; (b) Absorption difference spectrum and the corresponding refractive index changing spectrum
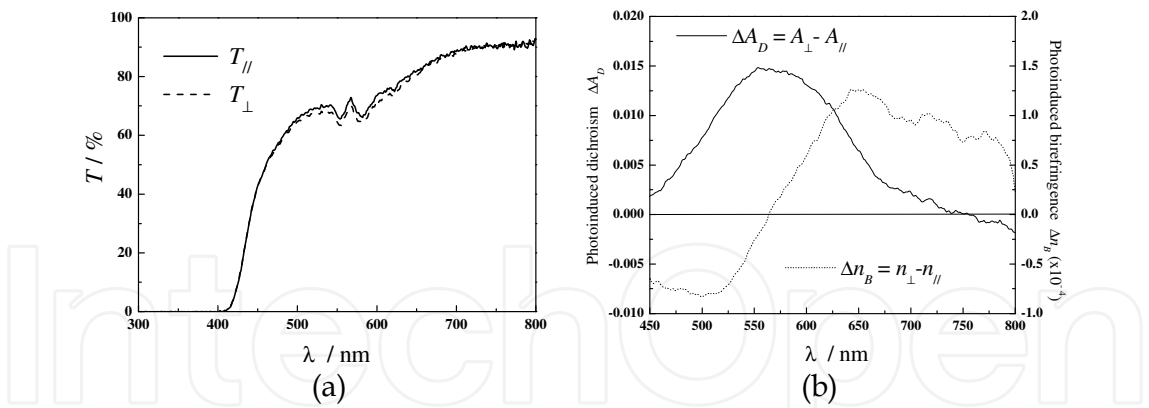
Fig. 11. Spectra of photo-induced anisotropic properties of Indolyfulgimide /PMMA film excited by linearly polarized light: (a) Transmission spectra on directions parallel and perpendicular to exciting beam polarization; (b) Dichroism and birefringence spectra

From Fig.10a and Fig.11a, the photo-induced absorption changing spectrum $\Delta A(\lambda) = A_E(\lambda) - A_C(\lambda)$ and the photo-induced dichroism spectrum $\Delta A_D(\lambda) = A_\perp(\lambda) - A_{//}(\lambda) = \lg(T_{//}(\lambda)/T_\perp(\lambda))$ were obtained, which are shown as solid lines in Fig.10b and Fig.11b respectively. Assuming that ΔA and ΔA_D are zero outside of the band 300~800nm, the photo-induced refractive index changing spectrum $\Delta n(\lambda) = n_E(\lambda) - n_C(\lambda)$ and the photo-induced birefringence spectrum $\Delta n_B(\lambda) = n_\perp(\lambda) - n_{//}(\lambda)$ can be calculated according to the Kramers-Kronig relation [5], where n_E, n_C, $n_{//}$ and $n_\perp$ are the refractive indexes of E-form, C-form and of the film excited by linearly polarized light along the photo-induced extraordinary and ordinary axes, respectively. The calculated Δn, Δn_B are plotted as dot lines in Fig.10b and Fig.11b respectively. Kramers-Kronig relation can be satisfied during all the photochromic reaction progress, so at one wavelength λ, $\Delta n(\lambda)$ is proportional to $\Delta A(\lambda)$ and $\Delta n_B(\lambda)$ is proportional to $\Delta A_D(\lambda)$ at different exciting time. From the Fig.10b and Fig.11b, it can be seen that at 633nm in this sample, $\Delta n(633nm)/\Delta A(633nm)=0.00994$ and $\Delta n_B(633nm)/ \Delta A_D(633nm)=0.006115$.

2.5.3 Dynamics of photochromic and photo-induced anisotropy properties of the sample

The transmission growing up kinetics of the sample at 633nm were measured on the parallel and perpendicular directions to exciting beam polarization, when the C-form sample was being excited with 314mW/cm^2 and 157mW/cm^2 intensity linearly polarized 633nm He-Ne lasers (I_W) respectively, and an 1mW/cm^2 633nm laser beam is used as the testing beam (I_T), the optical setup and the results are shown in Fig.12 and Fig.13a. From Fig.13a, it can be seen that the photochromic reaction and photo-induced anisotropy progress of fulgide material is an optical cumulating progress, which just depending on the Exposure, so it is enough to consider just one exciting beam intensity condition for the analysis.
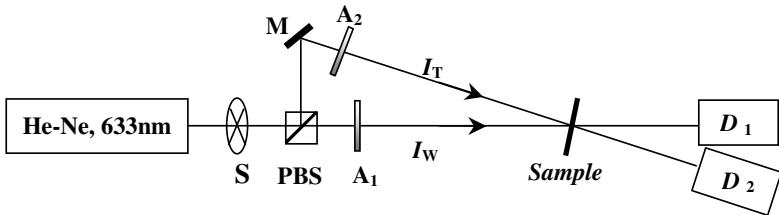

Fig. 12. Schematic of the experimental setup for measuring transmission kinetics.
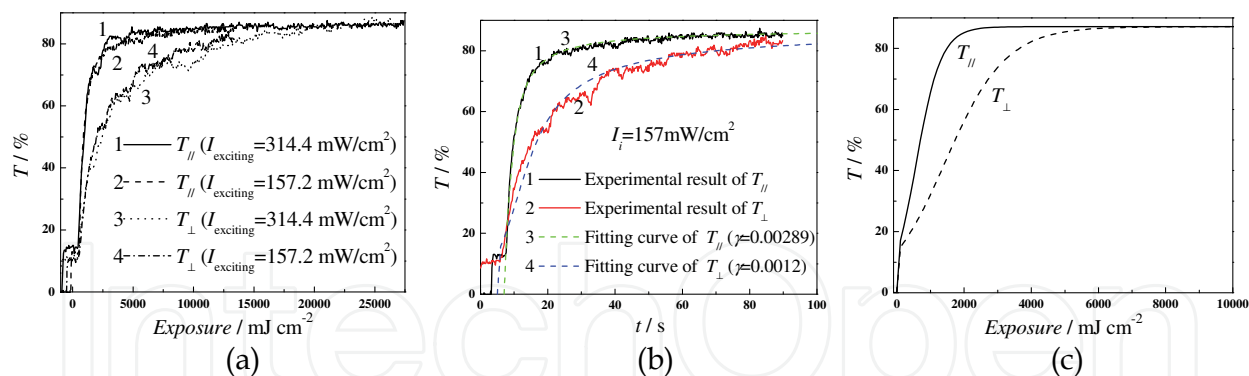
Fig. 13. Photo-induced anisotropic transmission curves of Indolyfulgimide/PMMA film on the directions parallel or perpendicular to exciting beam polarization depending on the exposure or erasing time: (a) Experiment curves measured at different exiting beam intensity; (b) Simulation of experimental results; (c) Calculated curves of uniformity light

For the analysis, we consider a fully bistable Fulgide system, neglecting side reactions like E-Z isomerization or aging effects. Using numerical calculation method [6], where the intensity Gaussian beam distribution of the He-Ne laser beam has been considered, the experimental curves were simulated (shown as the dash lines in Fig.13b) and the best fitting values $\gamma_{//}=0.00289 \text{cm}^2/\text{mJ}$, $\gamma_{\perp}=0.0012 \text{cm}^2/\text{mJ}$ were obtained.. Then the photo-induced anisotropic transmission curves of uniformity light are calculated like shown in the Fig.13c.

3. Holographic recording properties of one kind of indoly-benzylfulgimide/PMMA film

3.1 Kinetics of diffraction efficiency (DE)
3.1.1 Measurement set up

The system configuration for measuring the real-time hologram first order diffraction kinetics of the Fulgide film is schematically illustrated in Fig.14. A He-Ne laser (Melles Griot Inc., USA, 25-LHP-928, 632.8nm, 35mW, vertical linear polarized) is used to generate recording beams (object beam I_O and reference beam I_R) and readout beam (reconstruction beam I_C), and a laser diode LD (Power Technology Inc., USA, IQ2A18, 405nm, 10mW, vertical linear polarized) is used as the auxiliary light source (I_A) and erasing light source (I_E). The He-Ne laser beam is split into the I_O, I_R and I_C after beam splitter BS₁ and polarization beam splitter PBS, in which I_R and I_C are phase conjugated (counter-propagated) beams. The diffracted light I_D of I_C, diffracted by the dynamic holographic grating established by the interference between the I_O and I_R, will be phase conjugated with the I_O, whose power was real time detected by a digital power meter 'D' (United Detector Technology company, USA，11A Photometer / Radiometer, 254~1100nm, Imax=10mW, resolution is 0.01nW) and a digital oscilloscope 'O' (Tektronix company, USA, TDS3032, 300MHz, 2.5GS/s, 1mV) after reflected by the BS₂ (R47%). The I_O and I_R are symmetrically incident on the sample (Fulgide film), whose intersection angle $2\theta=16.5°$, so the recorded grating is a non-incline grating. Shutter S₁ and S₂ controls the exposure time of red and purple beams. The continuously adjustable attenuators A₁~A₃ are used to adjust the intensities of the waves, in this experiment $I_O=I_R=78.6 \text{mW/cm}^2$ and $I_C=0.786 \text{mW/cm}^2$ (i.e. $I_O:I_R:I_C=100:100:1$). This insures that the sub-reflection gratings formed by I_O and I_C as well as I_R and I_C can be ignored. The Quarter-wave plates Q₁~Q₄ and the polarizer P are

Polarisation of Object Light	Polarisation of Reference Light	Polarisation of Reconstruction Light	Polarization states of diffracted lights		+1st order diffraction efficiencies	
			+1	-1	Amplitude hologram $\eta_{A,+1}$	Phase hologram $\eta_{P,+1}$
$\updownarrow$	$\updownarrow$	$\leftrightarrow$	$\leftrightarrow$	$\leftrightarrow$	$(\tau_{1om}/2)^2$	$(\tau_{0om}\cdot J_1(\Psi_{1om}))^2$
		$\updownarrow$	$\updownarrow$	$\updownarrow$	$(\tau_{1em}/2)^2$	$(\tau_{0em}\cdot J_1(\Psi_{1em}))^2$
		$\circlearrowleft$	$\circlearrowleft$	$\circlearrowleft$	$\dfrac{(\tau_{1om})^2+(\tau_{1em})^2}{8}$	$\dfrac{\tau^2_{0em}\cdot J_1(\Psi_{1em})^2+\tau^2_{0om}\cdot J_1(\Psi_{1om})^2}{2}$
		$\circlearrowright$	$\circlearrowright$	$\circlearrowright$	$\dfrac{(\tau_{1om})^2+(\tau_{1em})^2}{8}$	$\dfrac{\tau^2_{0em}\cdot J_1(\Psi_{1em})^2+\tau^2_{0om}\cdot J_1(\Psi_{1om})^2}{2}$
$\circ$	$\circ$	$\leftrightarrow$	$\leftrightarrow$	$\leftrightarrow$	$(\tau_{1Mm}/2)^2$	$(\tau_{0Mm}\cdot J_1(\Psi_{1Mm}))^2$
		$\updownarrow$	$\updownarrow$	$\updownarrow$	$(\tau_{1Mm}/2)^2$	$(\tau_{0Mm}\cdot J_1(\Psi_{1Mm}))^2$
		$\circlearrowleft$	$\circlearrowleft$	$\circlearrowleft$	$(\tau_{1Mm}/2)^2$	$(\tau_{0Mm}\cdot J_1(\Psi_{1Mm}))^2$
		$\circlearrowright$	$\circlearrowright$	$\circlearrowright$	$(\tau_{1Mm}/2)^2$	$(\tau_{0Mm}\cdot J_1(\Psi_{1Mm}))^2$
$\leftrightarrow$	$\updownarrow$	$\leftrightarrow$	$\updownarrow$	$\updownarrow$	$(\tau_{1eo}/2)^2$	$(\tau_{0eo}\cdot J_1(\Psi_{1eo}))^2$
		$\updownarrow$	$\leftrightarrow$	$\leftrightarrow$	$(\tau_{1eo}/2)^2$	$(\tau_{0eo}\cdot J_1(\Psi_{1eo}))^2$
		$\circlearrowleft$	$\circlearrowleft$	$\circlearrowleft$	$(\tau_{1eo}/2)^2$	$(\tau_{0eo}\cdot J_1(\Psi_{1eo}))^2$
		$\circlearrowright$	$\circlearrowright$	$\circlearrowright$	$(\tau_{1eo}/2)^2$	$(\tau_{0eo}\cdot J_1(\Psi_{1eo}))^2$
$\circ$	$\circ$	$\leftrightarrow$	$\circlearrowleft$	$\circlearrowright$	$(\tau_{1eo})^2/2$	$(\tau_{0eo}\cdot \sin\Psi_{1eo})^2/2$
		$\updownarrow$	$\circlearrowleft$	$\circlearrowright$	$(\tau_{1eo})^2/2$	$(\tau_{0eo}\cdot \sin\Psi_{1eo})^2/2$
		$\circlearrowleft$	$\circlearrowleft$	—	$(\tau_{1eo})^2$	$(\tau_{0eo}\cdot \sin\Psi_{1eo})^2$
		$\circlearrowright$	—	$\circlearrowright$	0	0

Table 1. DWPS and DE of different kinds of polarization holograms

used to change the polarization states of the waves, here four different polarization recording: parallel linearly polarization recording, parallel circularly polarization recording, orthogonal linearly polarization recording and orthogonal circularly polarization recording were studied, everyone was constructed by horizontal, vertical, left circular and right circular polarized four kinds of lights like shown in table 1.
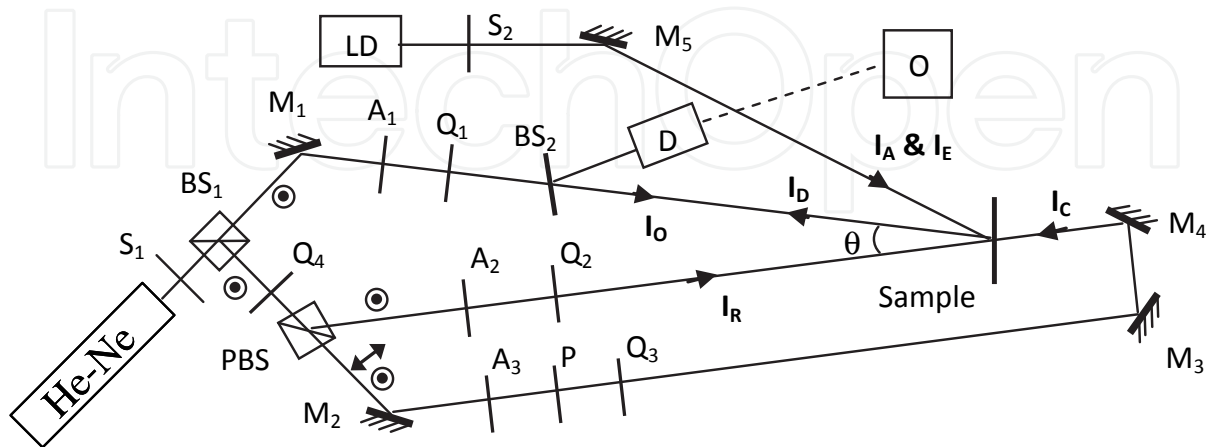
Fig. 14. Schematic of the experimental setup for measuring real-time polarization hologram diffraction kinetics.

3.1.2 Measurement results

In four kinds of polarization recording, and different polarization reading, the diffracted wave polarization states (DWPS) obtained in the experiments are shown in table 1 and the measured kinetic first order diffraction efficiency (DE) curves $\eta_{+1} \sim t$ are shown in Fig.15(a,c,d,e). From them the curves of the conditions when I_C has same polarization state with I_R were compared in Fig.16a. It can be seen that there exist an optimal exposure about $2 \times 78.6 \text{mW/cm}^2 \times 3.75\text{s} \approx 590 \text{ mJ/cm}^2$.

3.1.3 Theoretical analysis

DE dynamic curves at 633nm of different kinds of holograms recorded in the sample can be calculated from the photochromic and photo-induced anisotropic properties of the sample written in section 2.5, by using the DE formulas written in Table 1 [7]. Where the $(\tau_e\text{-}\tau_o)$ indicate the photoinduced anisotropy of the sample under the irradiation of linearly polarized light at some exposure, $(n_e\text{-}n_o)$ indicate the corresponding birefringence, $\tau_M=(\tau_e+\tau_o)/2$ indicate the amplitude transmission of the sample for nonpolarized light or circularly polarized light at this time (at the area of light strips in the interference field), τ_m indicates the amplitude transmission of the sample before the illumination of light (at the area of dark strips in the interference field, isotropy), τ_E and τ_C indicate the amplitude transmission of the E-form and C-form sample respectively, n_M, n_m, n_E and n_C indicate the corresponding refractive index of the sample, $\Psi_i=k_0 \cdot n_i \cdot d$ (i=e, o, M, m, E, C), and it is defined that $\tau_{0ij}=(\tau_i+\tau_j)/2$, $\tau_{1ij}=(\tau_i\text{-}\tau_j)/2$, $\Psi_{0ij}=(\Psi_i+\Psi_j)/2$, $\Psi_{1ij}=(\Psi_i\text{-}\Psi_j)/2$ (i, j = e, o, M, m, E, C).The theoretically calculated diffraction efficiency kinetics curves of parallel linearly polarization hologram are shown in Fig.15b. In parallel circularly polarization recording hologram, the DE curves are same with each other for any kinds of polarized reconstruction light I_C, which

is also same with that of parallel linearly polarization hologram for circularly polarized I_C. In orthogonal linearly polarization recording hologram, the DE curves are also same with each other for any kinds of polarized I_C, which is shown in Fig.16b. For orthogonal circularly polarization recording hologram, when I_C has same polarization state with I_R ($\vec{O} \perp \vec{R} // \vec{C}$), the DE curve is shown in Fig.16b; when I_C has orthogonal polarization state with I_R, the DE is zero; when I_C is linearly polarized, the DE is half of that in $\vec{O} \perp \vec{R} // \vec{C}$ condition. The theoretical DE kinetics curves of different kinds of polarization recording holograms for I_C has same polarization state with I_R, are compared in Fig.16b.
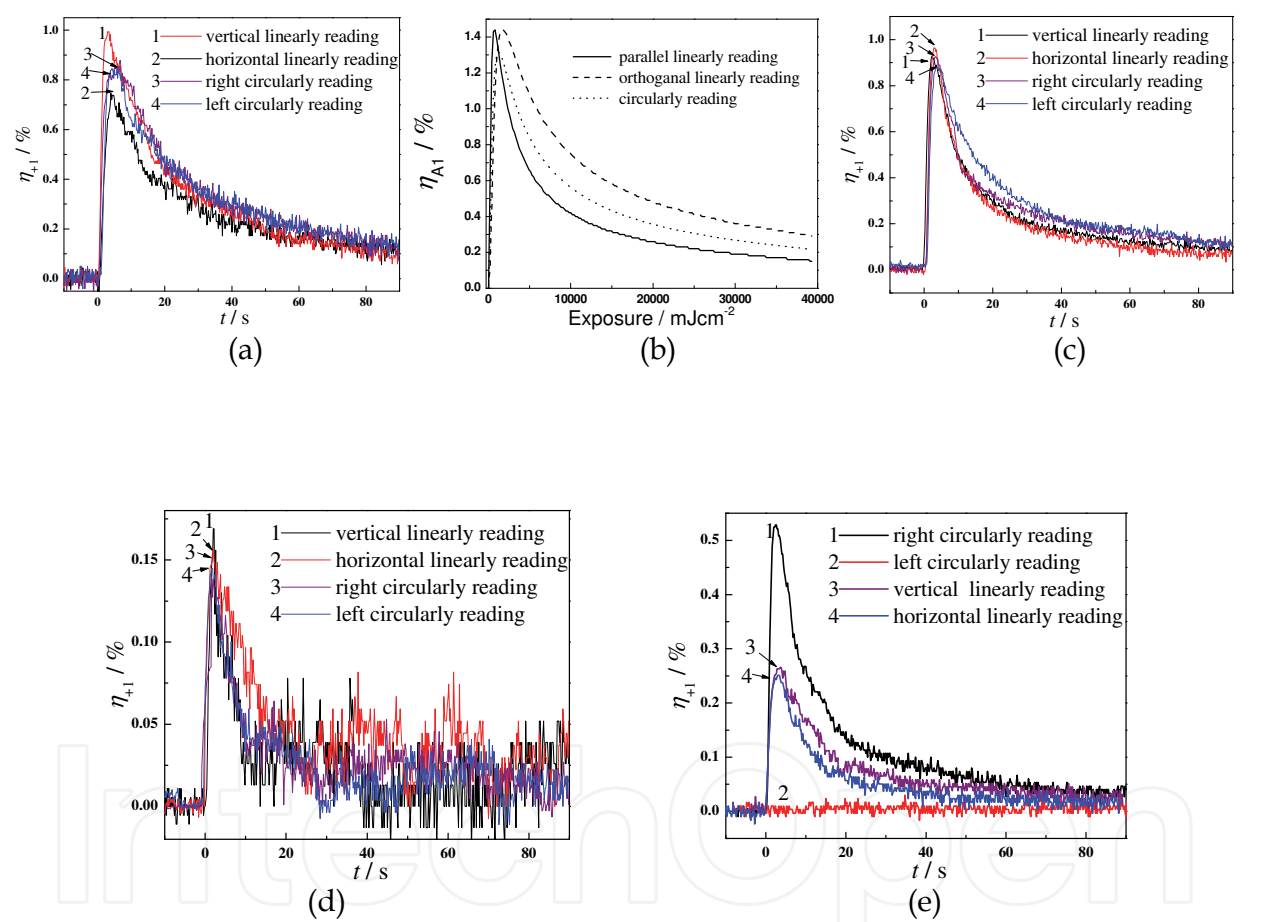
Fig. 15. The diffraction efficiency kinetics curves comparison of different kinds of polarization recording and different kinds of reading in Fulgide film: (a) Experimental results (ER) of parallel linearly polarization recording (b) theoretically calculated curves of parallel linearly polarization hologram (c) ER of Parallel circularly polarization recording; (d) ER of Orthogonal linearly polarization recording; (e) ER of Orthogonal circularly polarization recording
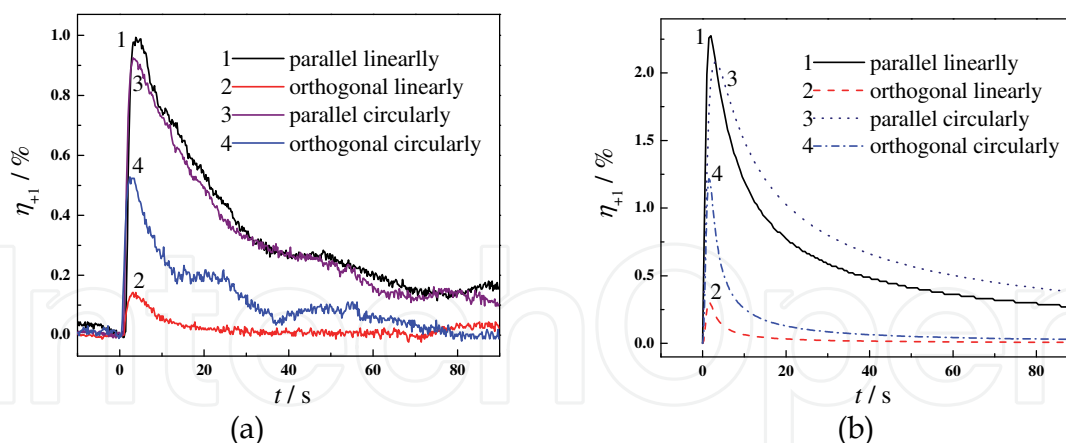
Fig. 16. The diffraction efficiency kinetics curves comparison of different kinds of polarization recording holograms in Fulgide/PMMA film written by Gaussian beams: (a) Experimentally measured results; (b) Theoretically calculated results

It can be seen that the maximum values' ratio of the measured values is basically coincide with the theoretically analyzed one. Only for parallel linearly polarization hologram, in the orthogonal linearly polarization reconstruction condition ($\vec{C} \perp \vec{O} // \vec{R}$), the diffraction efficiency is lower than parallel linearly polarization reconstruction condition ($\vec{C} // \vec{O} // \vec{R}$). It is because that, in calculation the affection of $\vec{C}$ is not considered, which can be proved to be very small when the $I_C = I_O/100 = I_R/100$ comparing to the affection of non-linear absorption of the film, whose detail calculation progress will not be given here, where it also can be deduced that the reading beam affection is larger in $\vec{C} \perp \vec{O} // \vec{R}$ condition than in $\vec{C} // \vec{O} // \vec{R}$ condition.

And the theoretical results are larger than the experimental results, and the reaction is quicker (optimal exposures are about 590 mJ/cm² and 430mJ/cm² respectively in experimental results and theoretical results), this may be caused by: (1) the sample is not homogeneous, the density is different at different area; (2) the incidence angles of beams θ in the experiment are about 8.2°, so the intensities of them on the sample plane will be $\cos\theta \approx$ 0.9898 times of the values used in calculation; (3) the photoreaction rate constants used in calculation is a little bit larger than real ones.

And it can be seen that no matter during the ordinary holograph recording process in photochromic media, or during the polarization holograph recording process in photo-induced anisotropy media, there exits an overshooting peak in the diffraction efficiency, which then decays to a lower permanent level or also to zero. From the theoretical analyses, it can be deduced that is caused by the diminishing of fringe contrast mainly caused by the nonlinear saturation effects of photoisomerization process and photo-induced anisotropy process. In experiment, there also exit the diminishing of fringe contrast caused by a photochemically active readout beam and unequal intensities of object and reference waves. It can be theoretically calculated that the effects of them show very smaller than that of the nonlinear saturation effects, which will not be given here.

3.2 The DE spectra of different kinds of holograms in fulgide film

Suppose that the holographic recording is a linearity recording, from the spectra of ΔA, Δn, ΔA_D and Δn_B, shown in Fig.3b and Fig.4b, using the DE formulas of different kinds

of polarization holographies, shown in table 1, the DE spectra of the ordinary holograms (i.e. parallel circularly polarization recording) and polarization holograms (orthogonal linearly and orthogonal circularly polarization recording) can be calculated, which are shown in Fig.17, where the solid line, dot dash lines and dash lines indicate the η_{total}, η_A and η_P respectively. It can be seen that at 450nm and 700nm the diffraction efficiencies are higher, while the absorption is very small, where the recorded information can be read out without any photochromic reaction, i.e. the non-destructive reconstruction can be realized.
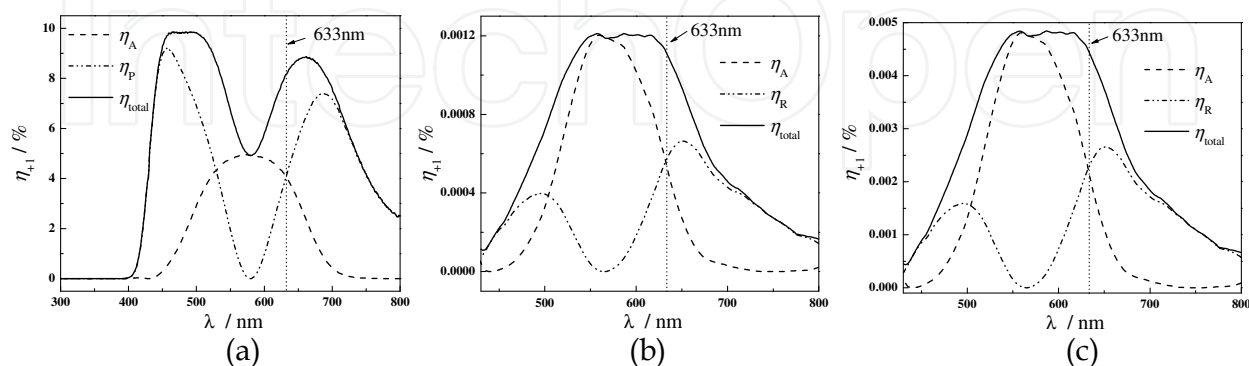
Fig. 17. Diffraction efficiency spectra of the (a) Ordinary holography; (b) Orthogonal linearly polarization holography; (c) Orthogonal circularly polarization holography

3.3 Effects of auxiliary light and object reference ratio to DE of Fulgide film

No matter during the ordinary holograph recording process in photochromic media, or during the polarization holograph recording process in photo-induced anisotropy media, there exits an overshooting peak in the diffraction efficiency, which then decays to a lower permanent level or also to zero, because of the diminishing of fringe contrast caused by a photochemically active readout beam, unequal intensities of object and reference waves and the nonlinear saturation effects of photoisomerization process and photo-induced anisotropy process. It is known that in ordinary holographic recording, this decreasing process can be eliminated by illuminating the hologram with a uniform control beam that has the effect of molecular back-conversion photochrome [8]. It was found that in polarization holographic recording, this method also can be used [8]. In this section experiments done with an ordinary hologram and a polarization hologram recorded in a 3-indoly-benzylfulgimide/PMMA film at 633 nm have shown that a control beam at 405 nm can increase the stable-state diffraction efficiency, thus, allowing to decrease the rigorous requirements on the recording time, the object reference ratio and the reading beam intensity in the holographic recording. The affections of object reference ratio (ORR) to DE of different holograms recorded in 3-indoly-benzylfulgimide/PMMA film were also measured.

The optical set up shown in Fig.14 is also used in this experiment. Here recording with linearly polarized beams with identical states of polarization (scalar hologram) and recording with circularly polarized beams with orthogonal states of polarization (polarization hologram) were studied. The holograms were reconstructed by light with the same polarization as the reference light.

3.3.1 Measurement of the effect of polarization of the auxiliary light

First the effect of the state of polarization of the auxiliary light was studied. The diffraction efficiencies of two different kinds of holographs were measured when the 405nm auxiliary beam is vertical and horizontal linearly polarized respectively. And the results show that the

effect of the polarization of the auxiliary light is very small, the regular is: in the parallel linearly polarized recording the diffraction efficiency is slightly higher when the auxiliary light is parallel to the polarization state of the recording lights than orthogonally polarized; in the orthogonal circularly polarized recording the polarization direction of the auxiliary light nearly have no effects. So we choose the vertical polarization for the LD laser in the below experiments.

3.3.2 Measurement of the effect of the intensity of the auxiliary light

Under the irradiation of different intensity auxiliary lights, the diffraction efficiencies of two kinds of holograms were measured in real time. The kinetics curves of the diffraction efficiencies of parallel linearly polarized recording and the maximum values and stable values contrasts are shown in Fig.18(a,b), and the results in orthogonal circularly polarized recording are shown in Fig.18(c,d).

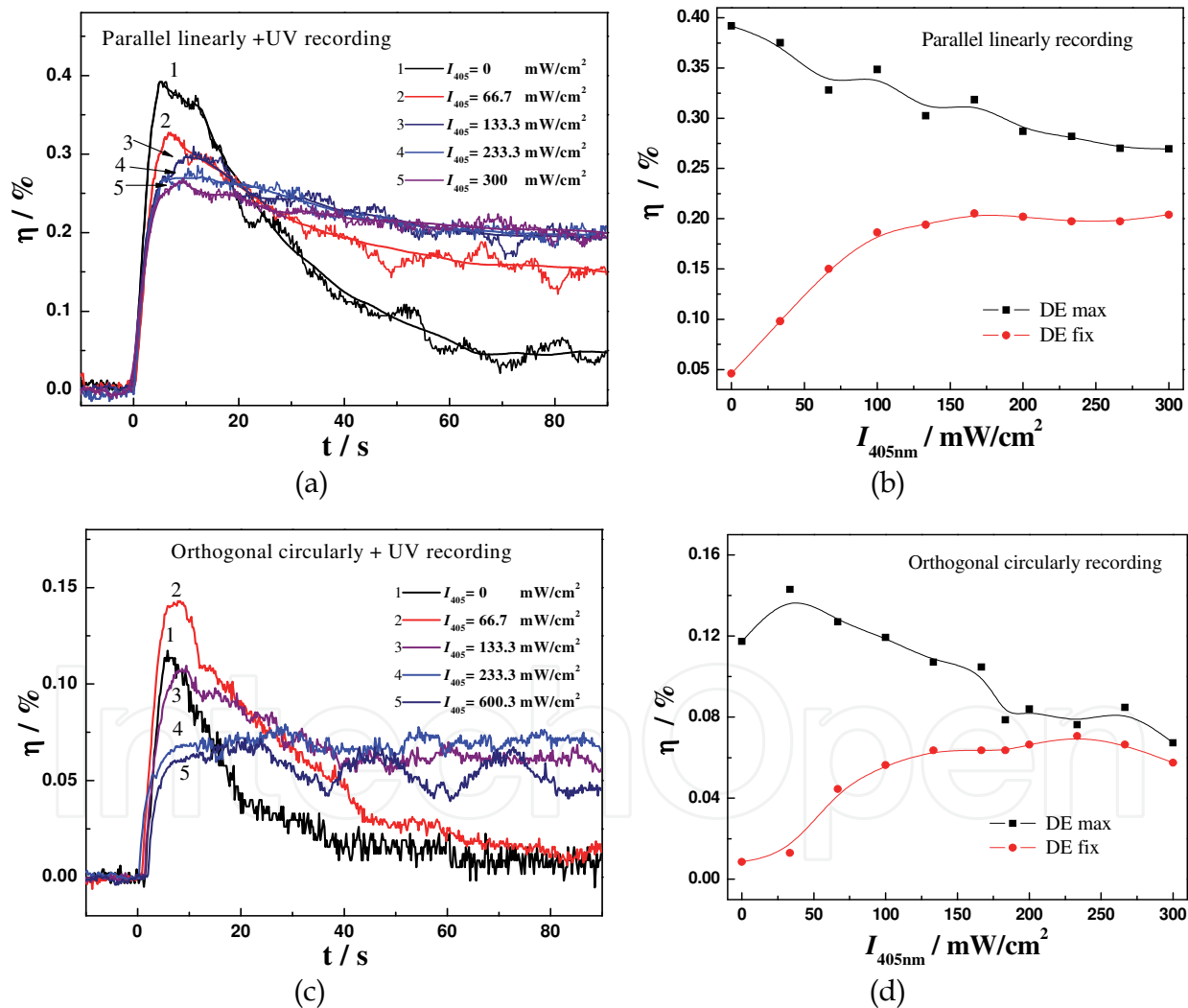Fig. 18. (a,b): Diffraction efficiencies of parallel linearly polarization holograph under the irradiation of different intensity auxiliary lights: (a) kinetics curves; (b) maximum values and stable values compare. **(c,d):** Diffraction efficiencies of orthogonal circularly polarization holograph under the irradiation of different intensity auxiliary lights: (c) kinetics curves; (d) maximum values and stable values compare

These results show that, under the irradiation of auxiliary light, the diffraction efficiency stable-state values can be increased no matter in ordinary hologram or in polarization hologram, and there exits an optimal intensity, under which the maximum stable-state diffraction efficiency can be obtained. When $I_O=I_R=78.6\text{mW/cm}^2$ and $I_C=0.786\text{mW/cm}^2$, in the parallel linearly recording, the optimal intensity of the purple light, is larger than 300mW/cm^2; in the orthogonal circularly recording, the optimal intensity of the purple light is about 233mW/cm^2. And it can be seen that, when there is no auxiliary light, the diffraction efficiency is depending on the exposure too much, there exits rigorous requirement on the recording time. But if turn on the auxiliary light, the requirement is decreased.

3.3.3 Measurement of the effect of the auxiliary light on the ORR requirement

In this experiment $I_O=78.6\text{mW/cm}^2$, $I_C=0.786\text{mW/cm}^2$ and $I_A=267\text{mW/cm}^2$ were used. In the conditions of with and without auxiliary light, the diffraction efficiencies of two kinds of holograms were measured at different intensities of reference light. The experimental results of parallel linearly polarization hologram and of orthogonal circularly polarization hologram are shown in Fig.19 and Fig.20 respectively. It can be seen that in all kinds of polarization hologram, no matter turn on the auxiliary light or not, the ORR has great effect on the diffraction efficiency. But in ordinary holography, with auxiliary light irradiation, the diffraction efficiency changing in the area near ORR=1:1 is much slower than without auxiliary light irradiation, so the rigorous requirement on ORR can be decreased. In the polarization holography, when the reference beam intensity is a little bit higher than that of object beam, the diffraction efficiency will be maximum, the reason is currently unclear and is a subject of further investigation.

3.4 Dependence of DE on the reading beam incidence angle

The angular selectivity of the sample (*i.e.* the dependence of DE on the reading beam incidence angle) was measured, and the experimental set-up is shown in Fig.21. A 650nm LD is used as the recording and reading light source, and a 405nm LD is used as the erasing light source. Adjustment of coherence was made by creating a Michelson interferometer. The 650nm laser was first adjusted perpendicularly to the face of the beam-splitter cube, and then the transmitted and reflected beams intersect with each other on the sample after reflected by the mirrors. The interference fringes were tuned for optimum contrast by moving one of the mirrors (M2) with a translation stage. The two writing beams are symmetrically incident on the sample (Fulgide film), whose intersection angle $2\theta_B=10°$ corresponding to a grating spacing $\Lambda = 3.73$ μm, so the recorded grating is a non-incline grating, and the incidence angle of object light (signal light) and reference light are $\theta_s=-5°$ and $\theta_r=5°$ respectively. The sample is placed on the precision rotary platform (M-062 model, PI company, Germany), and the recording point of the hologram in the sample is on the shaft of platform. So when the platform is rotated, the recording point does not move. The continuously adjustable attenuators $A_1\sim A_2$ are used to adjust the intensities of the waves, in this experiment $I_O= I_R= 75\text{mW/cm}^2$ and $I_C=0.1875\text{mW/cm}^2$ (*i.e.* $I_O:I_R:I_C =400:400:1$). By observing the spots on the screen behind the sample, the best exposure time can be determined (see the next Section). Before reconstruction, the sample was rotated to one direction 20°. In the reconstruction time, the platform is rotated to the opposite direction

$40°$ with a uniform speed. The diffracted light was real time detected by a digital power meter and a digital oscilloscope. Measurement result is shown in Fig.22 as solid line, and the dashed line is its theoretical fitting curve by the formula $y=y_0 \cdot \text{sinc}^2(ax)$.
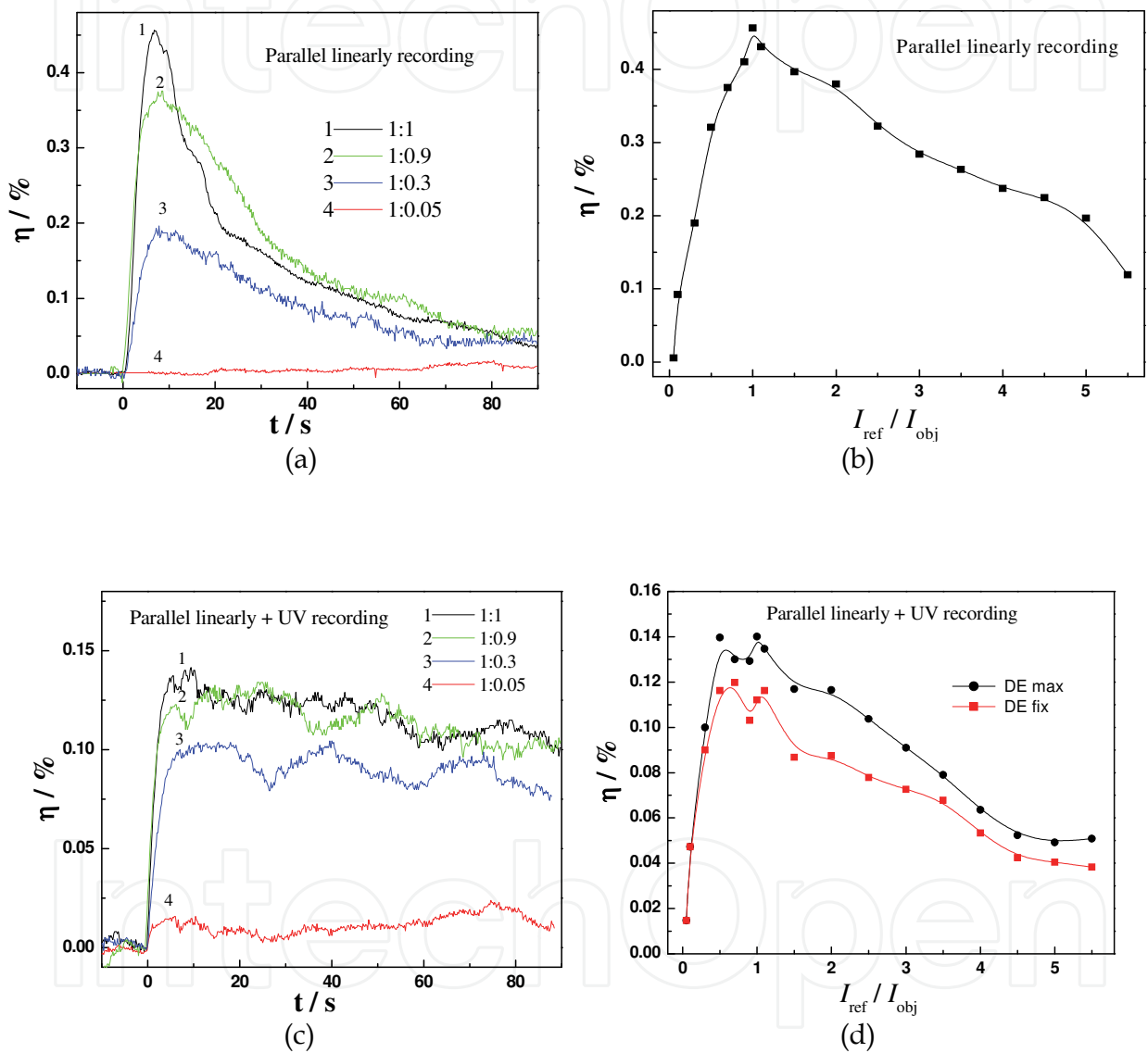
Fig. 19. The diffraction efficiency of parallel linearly polarization holograph recording at different ORR: (a) kinetic curves (*without auxiliary light*); (b) maximum values compare (*without auxiliary light*); (c) kinetic curves(*with auxiliary light*); (b) maximum values and stable values compare (*with auxiliary light*)
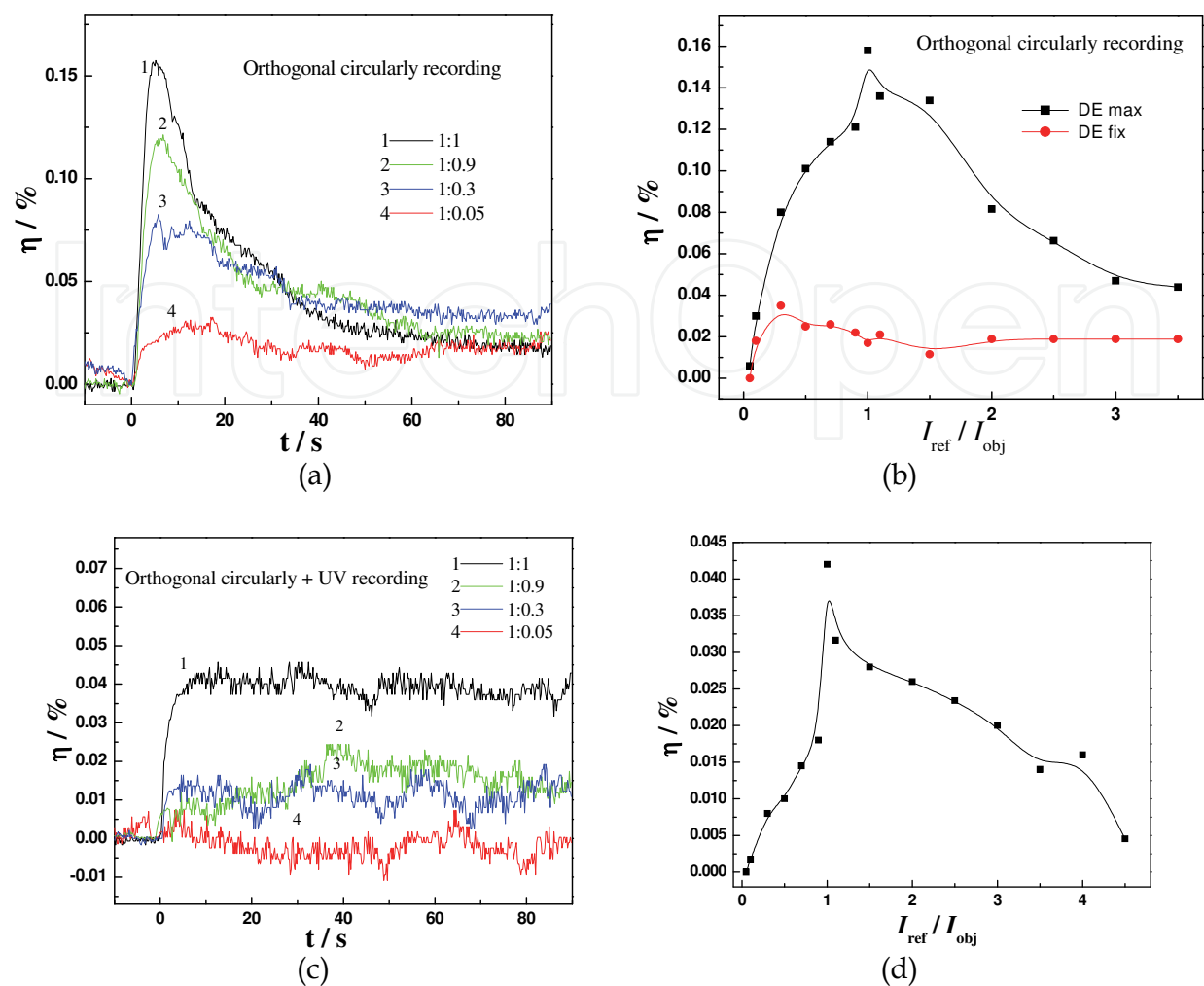
Fig. 20. The diffraction efficiency of orthogonal circularly polarization holograph recording at different ORR: (a) Kinetic curves(*without auxiliary light*); (b) maximum values and stable values compare(*without auxiliary light*); (c) Kinetic curves (*with auxiliary light*); (b) stable values compare (*maximum value basically same with the stable values, with auxiliary light*)
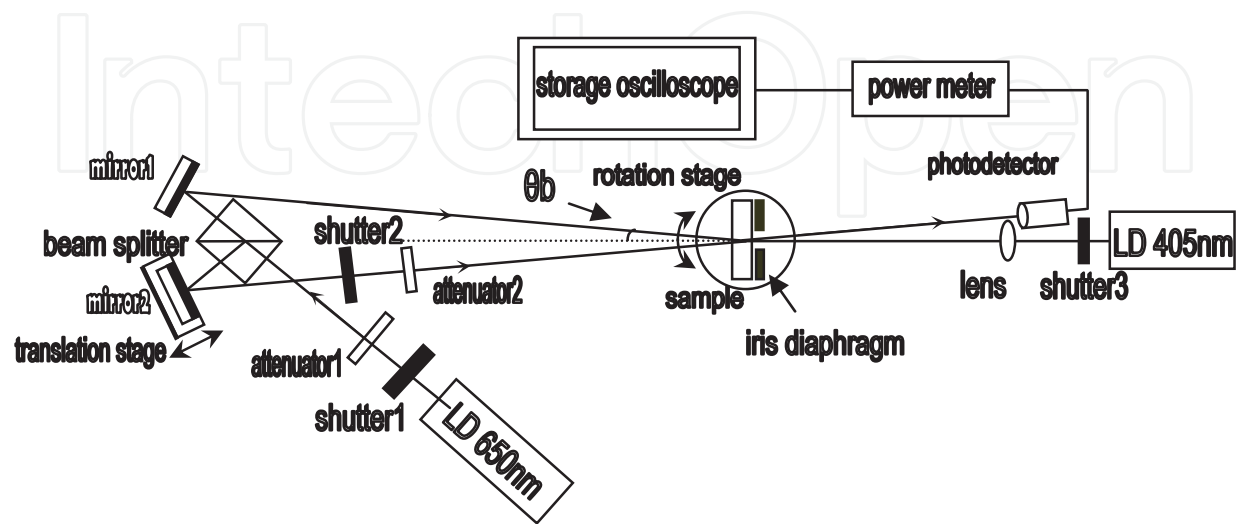
Fig. 21. The measurement set-up of angular selectivity of the sample
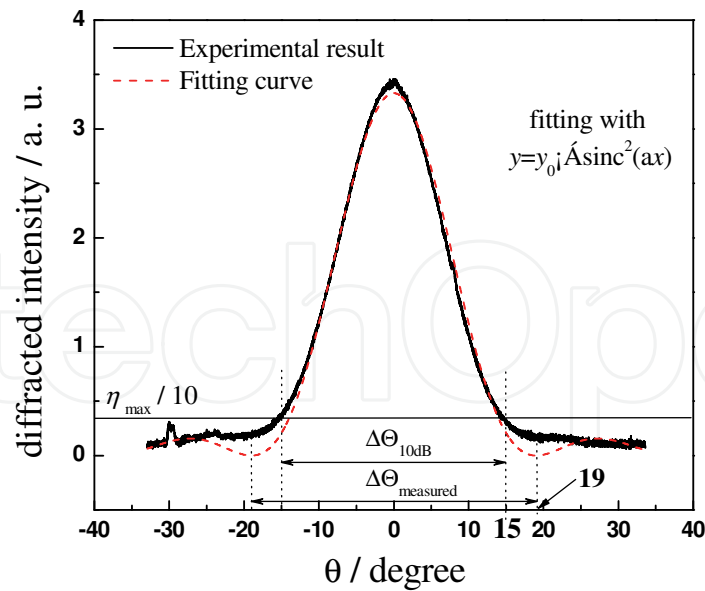
Fig. 22. The curves showing the DE dependence on the reading beam incidence angle

From the Fig.22, it can be seen that the angular selectivity $\Delta\Theta_{measured}$=38°, if it is taken as the angle between the first minimum diffractions at both sides of the fitting curve's peak. But Side lobes do not exist in the experimental curve, so the angular selectivity can be taken as the angular width at the 1/10 of the maximum diffraction efficiency, $\Delta\Theta_{10dB}$=30°.

In theory[10], the angular selectivity of the gratings $\Delta\Theta_{calculated}$ is:

$$\Delta\Theta = \frac{2\sqrt{\pi^2 - \nu^2}\lambda}{\pi nd}\frac{\cos\theta_s}{|\sin(\theta_r - \theta_s)|} \qquad (1)$$

Where $\nu = \pi\Delta nd / (\lambda\sqrt{\cos\theta_r \cos\theta_s})$. In this experiment, the λ=650nm, the thickness of the sample is d=10μm, the refractive index of the sample is about n≈1.5, and for this sample at 650nm the refractive index difference between E-form and C-form is Δn≈1.84×10⁻² , so it can be calculated that $\Delta\Theta_{calculated}$≈27.3°.

It can be seen from the experimental value of angular selectivity is greater than the calculated value. One of the reasons is that, for this calculation the incident beam is considered as an infinite plane wave, however, the spot diameter is small in actual storage experiment. According to diffraction theory, the limited size of the beam would inevitably lead to an angle broadening, so the measured curves are broadened.

3.5 The spatial resolution measurement of fulgide film

In the reflection type holographic image storage (where the Ic is used as reference beam, shown in section 4.1), the angles between the two recording waves is 173°, so it is proved that this sample can store the gratings with spatial frequency of 6300lines/mm.

3.6 Measurement of the optimum exposure of the sample

From the diffraction dynamic curves, the optimum exposure can be obtained. From Fig.15 it can be seen that he optimum exposure of the Fulgide is 590mJ/cm², the similar data also can be obtained from the changing of the diffracted spots' pattern, details please see in Reference [9].

4. Holographic image storage in fulgide film

4.1 Reference beam reconstruction hologram and phase conjugated beam reconstruction hologram (including transmission type hologram and reflection type hologram)

4.1.1 Experiment methods

The experimental setups for non-collinear holographic storage are shown in Fig.23and Fig.24. Fig.23 is the experimental setup of reference beam reconstruction holography. Fig.24 is the experimental setup of conjugated beam reconstruction holography. In every one of these two optical setups, the transmission type holographic recording and reflection type holographic recording both can be realized.
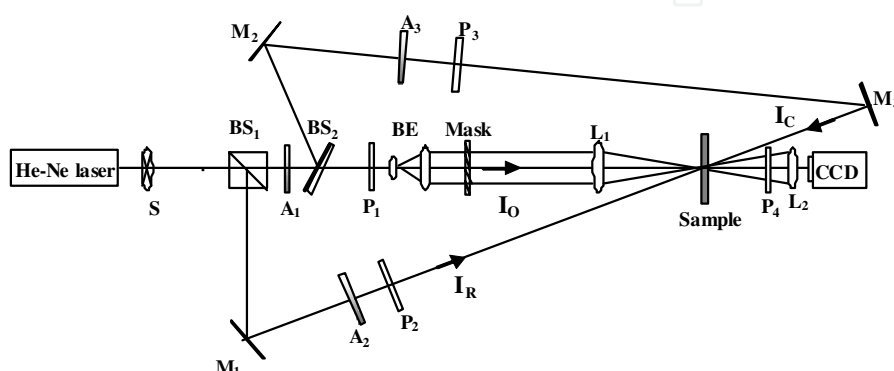
Fig. 23. Experimental setup of reference beam reconstruction holography
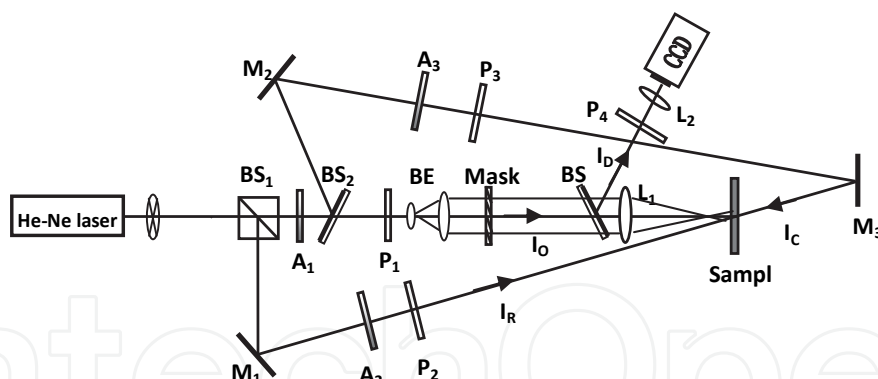
Fig. 24. Experimental setup of conjugated beam reconstruction holography

In Fig.23, the reference beam reconstruction is used. The nonpolarized He-Ne laser（632.8nm, 3mW）is split into three beams by beam splitters BS_1 and BS_2. The three beams are object beam I_O and two phase conjugated beams I_R and I_C. In transmission type holographic recording, reference beam is I_R，which is I_C in reflection type holographic recording. The signal of object beam is loaded by the Mask, which is imaged on the CCD's photosensitive surface by the positive lens L_1 and L_2. The focused I_O beam cross with reference beams after the focus of L_1, where a recording medium, the fulgide/PMMA film, has been placed for recording the hologram. In reconstruction process, using the reference beam as reconstruction beam, diffractive image is captured by the CCD. The shutter S is used to control the exposure time (the best exposure time is 10s in this experiment). The

continuously adjustable attenuators A_1, A_2 and A_3 are used to adjust the intensities of I_O, I_R and I_C. Polarizer P_1, P_2 and P_3 are used to adjust the polarization states of I_O, I_R and I_C. Polarizer P_4 in front of CCD is used to filter scattered light. For the ordinary holographic storage the Polarizers are not used. The intensities of object wave and reference wave are both 6mW/cm^2 in experiment. The angles between the two recording waves are 7° and 173°. The intensity of reconstruction beam is 60μW/cm^2. And the diameter of hologram is about 2mm.

In Fig.24, the phase conjugated beam is used as reconstruction beam. I_R and I_C are conjugate with each other. For transmission type holographic recording, reference and reconstruction beams are I_R and I_C respectively, which are exchanged with each other, for reflection type holographic recording experiment. Diffracted beam I_D is conjugated with object beam I_O. After being reflected by BS_3, the diffracted image can be detected by CCD real-timely. Other conditions are same with that of set up shown in Fig.23.

4.1.2 Results and discussions

4.1.2.1 Transmission type hologram and reflection type hologram

In Fig.25, the reconstructed images of parallel linearly polarized transmission type hologram and reflection type hologram (recorded in setup shown in Fig.23) are shown.

(a)   (b)
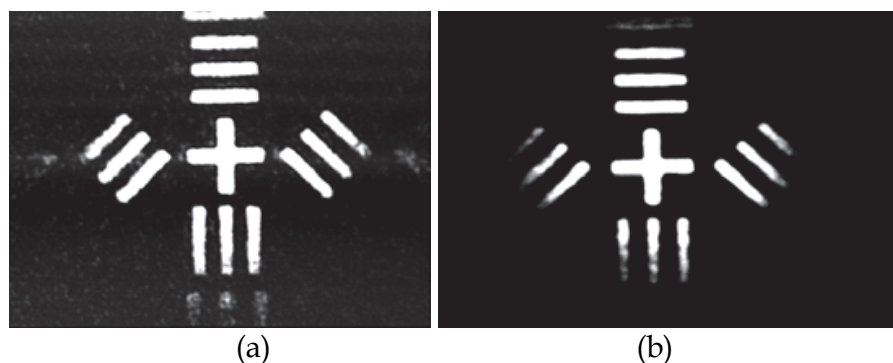
Fig. 25. The reconstructed images of parallel linear polarized transmission hologram and reflection hologram: (a) reconstructed image of transmission recording hologram; (b) reconstructed image of reflection recording hologram

It can be seen that: compared with transmission-type hologram, reflection-type hologram has higher SNR. This is because that the noise in the reconstructed image of transmission-type hologram is come from the forward scattering, but that of reflection-type holographic recording hologram is come from the backward scattering. Usually the forward scattering is always larger than backward scattering, so the reflection-type hologram has smaller noises. But reflection-type hologram has lower diffraction efficiency.

4.1.2.2 Reference beam reconstruction hologram and phase conjugated beam reconstruction hologram

In Fig.26, the reconstructed images of reference beam reconstruction hologram and conjugated beam reconstruction hologram are shown. It can be seen that: compared with reference beam reconstruction, the phase conjugated beam reconstruction can effectively correct the phase aberration caused by the mis-adjustment of optical setup and the real-time detection of the changing progress of the diffraction image can be realized.

(a)   (b)

Fig. 26. Reconstructed images of (a) reference beam reconstruction hologram (Phase aberration image) and (b) conjugated beam reconstruction hologram (Corrected image)

4.2 Fraunhofer hologram and Fourier transform hologram

According to the different arrangement of optical setup, holograms can be divided into Fresnel hologram, Fraunhofer hologram, Image plane hologram, Fourier transform hologram and quasi-Fourier transform hologram etc. In which Fraunhofer hologram and Fourier transform hologram are recorded here, the optical setups are shown in Fig.27 and Fig.28.
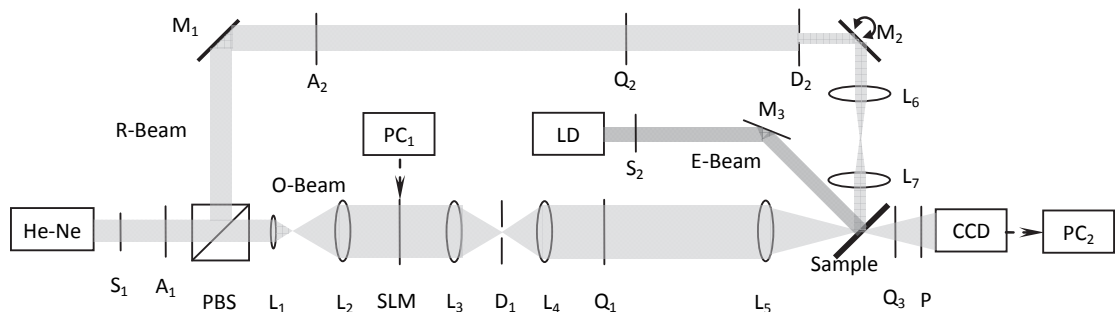
Fig. 27. Fraunhofer angular multiplexing holographic storage experimental setup
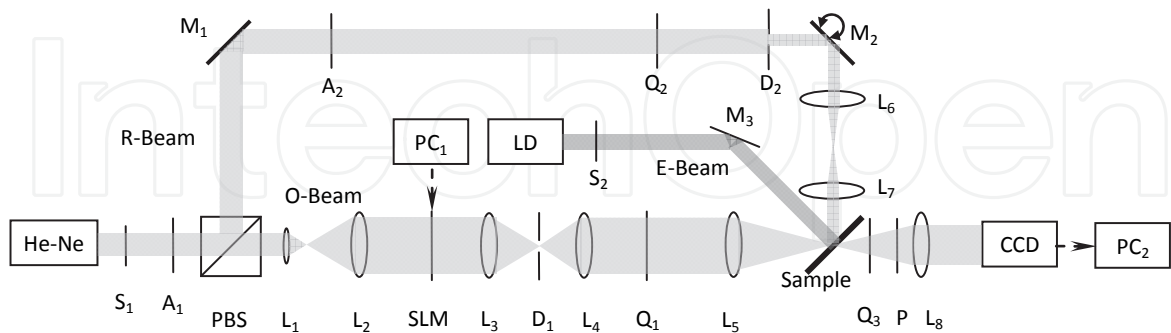
Fig. 28. Fourier transform angular multiplexing holographic storage experimental setup

It can be seen that in two optical setups, there are many common things, difference exist in finally imaging set up in the object beam path. In both setups, a He–Ne laser (633nm, 3mW) is used for recording and read-out beams. A diode laser (405nm, 10mW) is used as an erasing beam. Shutter S_1 and S_2 controls the exposure time and erasing time respectively. The continuously adjustable attenuators A_1 and A_2 are used to adjust the intensities of the object,

reference, and readout waves. The nonpolarized He–Ne laser is split (1:1) into two beams, a horizontally polarized object wave (O-Beam) and avertically polarized reference wave (R-Beam), by a polarization-sensitive beam splitter (PBS). Lenses L_1 and L_2 in the object beam path comprise a beam expander. Located in the front focal plane of the Fourier transform lens L_3, the spatial light modulator (SLM) was positioned such that the encoded data are loaded from the computer PC_1. The polarization state of the object wave becomes vertical after passing through the SLM. Diaphragm D1 is placed in the spatial frequency spectrum plane of the 4f system composed of L_3 and L_4, which is used to filter high-order diffractive waves, so on the back focal plane of L_4 the object image without grid structure to be recorded can be obtained. In the reference beam path, lenses L_6 and L_7 comprise a 4f system. Rotatable mirror M_2 is located at the focal plane of L_6, which is used to perform angular multiplexing (detail see the section 4.7.2). The angle between the object wave and the normal of the sample and the angle between the reference wave and the normal of the sample are both 45°. Quarter-wave plates Q_1, Q_2, and Q_3 are used to change the polarization states of the recording, read-out, and diffracted waves. Polarizer P is used to filter scattered light.

In the Fourier transform holographic storage experiment, the imaging system is another 4f system composed of lens L_5 and L_8. The object image to be stored located in the front focal plane of L_5 and the CCD is placed in the back focal plane of L_8. The fulgide film is placed on the spectrum plane of the system to record the Fourier transform holograms.

Only a difference of a quadratic phase factor occurs between Fraunhofer diffraction and Fourier transform. So when objects (or images to be stored) placed anywhere around the imaging lens the Fraunhofer hologram can be obtained. Here in the Fraunhofer holographic storage experiment, the image to be stored placed at about two-focal-distance before the imaging lens L_5, so the upside down same size image of the object will be formed at about two-focal-distance after the L_5, where is also the CCD photosensitive surface. Fulgide films were still near the back focal plane of L_5, so the size of the hologram is small, narrow laser beams can be used as reference beam and reconstruction beam.

Compared with Fraunhofer hologram, Fourier-transform hologram has small recording spot, higher storage density and the 4f system has better imaging quality than the single-lens. But because of the small recording spot, the diffracted light is weaker, which can be stronger when stronger reconstruction light is used, however the erasing effect will be sharpen up. The experiment results are shown in Fig.29, here will not be given individually.

4.3 The holograms with different polarization recording waves

In Section 3.1 the diffracted wave polarization states (DWPS) and the diffraction efficiencies (DE) of different polarization holograms recorded in a 3-indoly-benzylfulgimide /PMMA film are given. In this section, different polarization holographic image storages are realized in this film. Experimental setup as shown in Fig.28, four kinds of polarization holograms, like the parallel linearly polarization hologram, parallel circularly polarization hologram, orthogonal linearly polarization hologram and orthogonal circularly polarization hologram, are recorded, the Q_1, Q_2 are used to adjust the polarization states of O-beam and R-beam. The polarization state of scattering noise is similar to that of the original reconstruction light. And in the orthogonal polarization if the reference beam itself is used as the reconstruction light, the DWPS is orthogonal to the polarization state of reconstruction light, so using Q_3 and P the scattering noise can be filtered.

Fig.29 shows the comparison of retrieval diffractive images with different polarization recording waves on the fulgide film, when reconstruction beams has same polarization state with reference beams. It can be seen that these results are same with the measured results shown in Section 3.1. When the intensities of recording wave and readout wave are certain, the parallel linear polarization hologram has the highest DE, the parallel circular polarization hologram followed and the orthogonal circularly polarization hologram has the lowest DE. But in parallel polarization holograms, the scattering noises cannot be filtered, so their signal-to-noise-ratios (SNR) are lower. In orthogonal polarization holograms, the scattering noise can be filtered, so their SNRs are high.

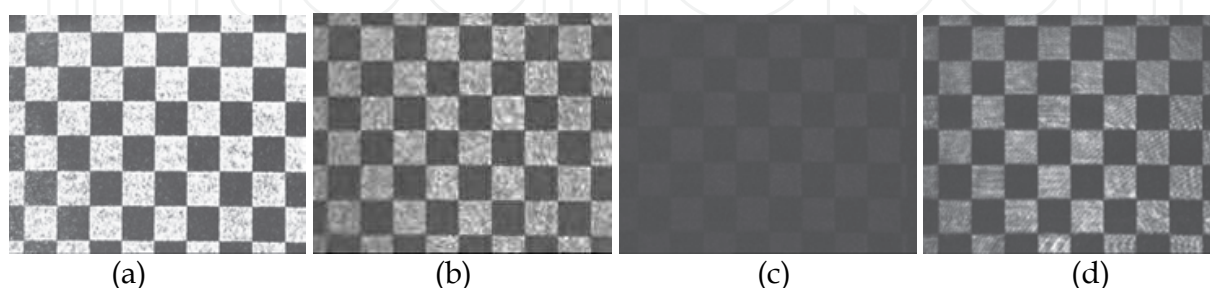| (a) | (b) | (c) | (d) |

Fig. 29. Results of holographic storage experiments with different polarization recording waves on Fulgide film: (a) parallel linear polarization recording; (b) parallel circular polarization recording; (c) orthogonal linear polarization recording; (d) orthogonal circular polarization recording

4.4 Fourier transformation orthogonal circular polarization holographic optical data storage

Orthogonal circular polarization hologram has higher DE and high SNR. Fourier transformation hologram has high storage density. So Fourier transformation orthogonal circular polarization recording is chosen as the method of high density holographic data storage in the fulgide film. Optical setup as shown in Fig.28, the intensities of O-beam and R-beam are both about 14mW/cm², optimum exposure time is 10s, and erasing time is smaller than 5s. The encoded binary data images loaded on the SLM are translated by our developed software in PC_1 by reading the data stream of the computer file. The black pixel represents "0" and the white pixel represents "1". The marginal periodically distributed black–white pixels are used as a reference for locating the pixels in the data-decoding process. The diffracted images will be captured by CCD and send to PC_2, which can be successfully decoded and recovered to the original file without any errors. The holograms can be restored after erased by the violet light.

In Fig.30 shows the experimental results. The images are separately stored file, encoded binary monochromic image, retrieval diffractive image, decoded result, retrieved file, measurement of size of holographic image. The retrieval diffractive image that is clear is processed by decoding procedure, and the obtained retrieved file is same as the stored file. In the experiment, data size of each stored holographic page is 81×61 bits, and the size of hologram is 60μm×42μm. So the storage area density of $2×10^8$ bits/cm² is obtained. The nonhomogeneity and flaws of the surface of sample, misalignmen of optical elements or uncertainty of adjustment brings out some distortion of the diffractive image and error codes that can be reduced to the minimum by designing reasonable encoding and decoding procedures.

(a)   (b)   (c)

(d)   (e)   (f)
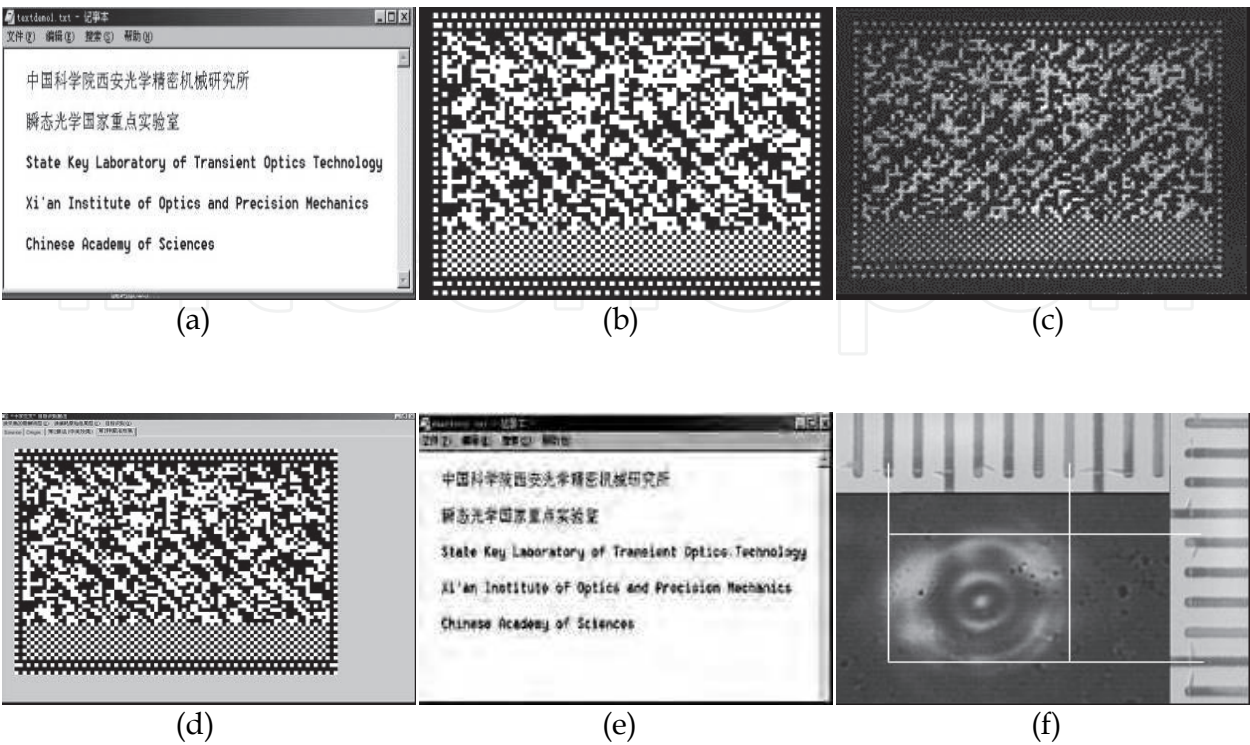
Fig. 30. Results of orthogonal circular polarization holographic optical data storage on BR-D96N film by Fourier transformation holographic method. (a) stored file; (b) encoded binary monochromic image; (c) retrieval diffractive image; (d) decoded result; (e) retrieved file; (f) measurement of size of hologram (one grid of the scale corresponds to 10μm).

4.5 Application of the auxiliary light effect in holographic image storage

The effect of auxiliary light is applied in real image holographic storage. An orthogonal linearly polarization transformation type holographic storage experiment setup was used, which is shown in Fig.31, where the reference light is also used as the reconstruction light and the diffuse reflection objects used as the target. A 633nm, 35mW vertically polarized He-Ne laser is used as the recording and reading light source, which has turned to the elliptically polarized light after a λ/4 plate, and then divided into two orthogonal polarized object light and reference light through the polarization beam splitter PBS. The polarizer P in front of the CCD was used to filter the scattered noises of reconstruction light. The 405nm LD laser is used as the eraser and auxiliary light source.

The images of the self-diffracted signal at three different instants are presented in Fig.32. The first image (Fig.32a) is taken at $E \approx E_{opt}$, whereas the second one (Fig.32b) corresponds to the case $E >> E_{opt}$ (auxiliary light is absent in both cases). As one can see, the recorded image is essentially lost through saturation, but it is restored at a significant level when the auxiliary control beam is turned on (Fig.32c), which proved that the diffraction efficiency can be increased and stabled when irradiated by an auxiliary light, and the rigorous requirement on the recording exposure is decreased.
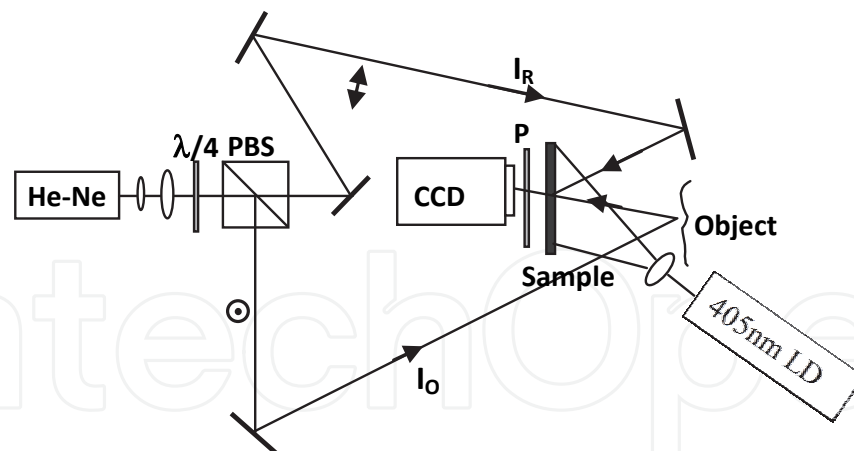
Fig. 31. Diffuse reflection object orthogonal linearly polarization transformation type holographic storage experiment setup
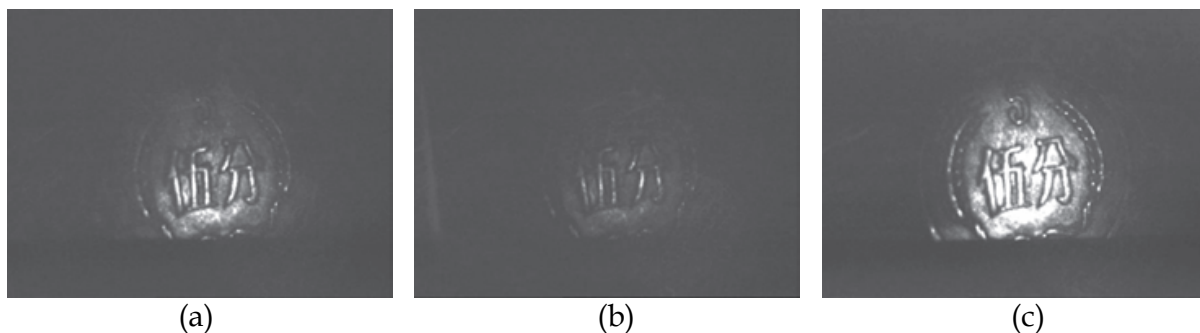

| (a) | (b) | (c) |

Fig. 32. The diffracted images of different holograms: (a) at $E{\approx}E_{\text{opt}}$, without auxiliary light; (b) at $E{>>}E_{\text{opt}}$, without auxiliary light; (c) exposed long enough time to be stable after the auxiliary light is turned on

4.6 Collinear hologram

In collinear holographic storage system, the experimental setup for rewritable collinear holographic image storage is shown in Fig.33(a). A He-Ne laser is used as the light source for recording and readout, and an ultraviolet laser diode is used as the light source for erasing. The non-polarized laser beam (632.8nm, 2mW) turns to be vertical polarized light by passing through the polarizer P, after being expanded and collimated by the lens L_1 and L_2. Then the beam is projected to transparent mask SLM (special light modulator). The pattern on the SLM used in recording process is shown in Fig.33(b), in which the center cross is the objective information pattern and the outer semi circles are the reference pattern. So the modulated laser beams by the SLM include both objective light (I_O) and reference light (I_R), whose intensities are respectively 318mW/cm² and 382mW/cm² (I_O:$I_R{\approx}$1:1.2). The patterns on the SLM are imaged on the CCD's photosensitive surface by the positive lens L_3 with focal length of 70mm. The I_O and I_C beams are focused and interfere with themselves at the focus of L_3, where a record medium, the BR film, has been placed for recording the hologram. In reconstruction process, only the outer semi circle patterns, as shown in Fig.33(c), is displayed on the SLM, where the object light pattern is covered. So the reconstruction light is same with the original reference light I_C, whose intensity is about 50mW/cm². And the retrieved diffractive image is captured by the CCD sensor. The

diameter of hologram stored in the media is about 0.2mm, as shown in Fig.34(a). In this system the shutter S is used to control the exposure time (the best exposure time is 13 second in this experiment). The continuously adjustable attenuator A is used to adjust the intensities of I_O and I_C (stronger for recording and weaker for readout). The diagram D, placed in front of the CCD, is used to filter the transmission light of I_C (zero-order diffraction), and to pass only the diffraction light I_D (+1 order diffraction). After erased by ultraviolet light, the holograms can be recorded repeatedly.
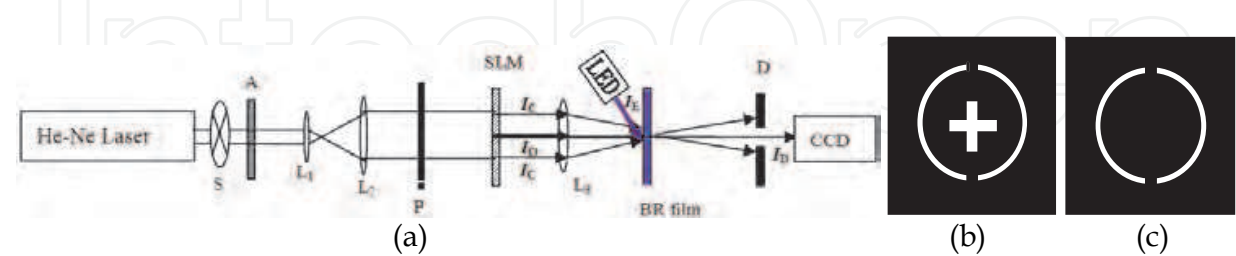

Fig. 33. Optical setup and the patterns displayed on the SLM in rewritable collinear holographic image storage; (a) Optical setup; (b) Recording process pattern; (c) Reading process pattern
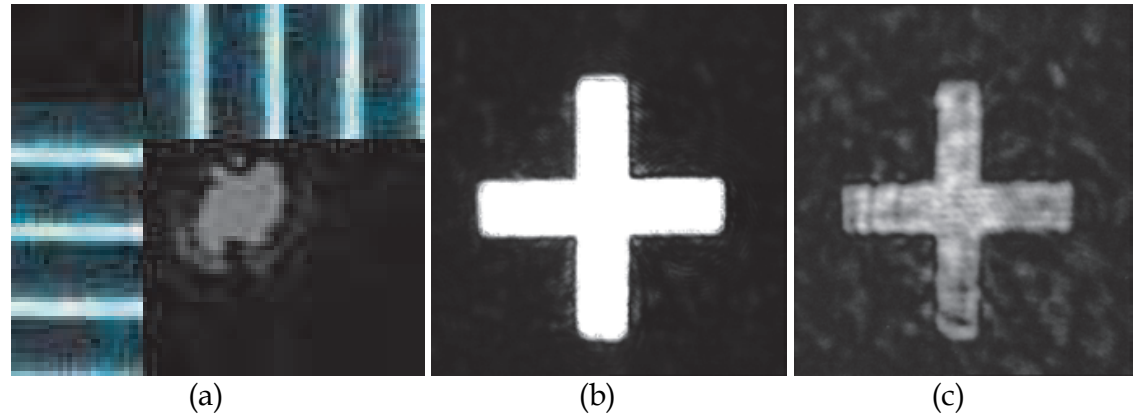

Fig. 34. Size measurement, objective image and reconstructed image of a collinear hologram stored in the media: (a) Size measurement (the scale is 100mm/div); (a) Original objective image; (b) Reconstructed image

In Fig.34(b,c), the results of parallel linear polarized collinear holographic storage experiment on a BR-D96N film are shown. Since the collinear hologram is recorded on the focus of lens, the size of the recording point is very small. So the diffracted light is very weak, which makes the scattering light of the reconstruction light entering into CCD (noises) look too much. In that case, the signal noise ratio (SNR) is very low. But this kind of noise can be filtered by using orthogonal polarization hologram recording technology. And high storage density can be realized in collinear holography because of its small recording area.

Comparing with traditional "two-beam interference recording method", the collinear holographic storage system has simpler optical setup and smaller volume. And in this system the demands for environment are lower, because the objective light and reference light pass through the same one path, in which there are same interferences from the vibration of environment, the change of temperature and the variety of airflow, those effects can be cut down.

4.7 Different kinds of multiplexing holographic storage

High-density high-capacity volume holographic multiplexing is one of the most attractive aspects of holographic data storage. The study on holographic multiplexing storage application of fulgide materials is very limited. Using the optical setups shown in Fig.28, polarization multiplexing, angular multiplexing and rotational multiplexing holographic experiments are carried out initially.

4.7.1 Polarization multiplexing holograms

Polarization multiplexing is based on the photo-induced anisotropic property of the material, at the same location of sample different kinds of polarization holograms are recorded. Todorov et al were first to show that two holographic recording could be stored independently inside the same film when using different combinations for the polarization states of the reference and the object beam during recording. Su et al presented a technique for polarization multiplexing in $LiNbO_3$. Koek et al have presented a technique for simultaneous readout polarization multiplexing in bacteriorhodopsin.

Here different kinds of polarization multiplexing holographic storage were realized in fulgide film, including linearly polarization multiplexing and circularly polarization multiplexing, optical setup as shown in Fig.28. In circularly polarization multiplexing experiments, at the same location of the sample parallel circularly polarization hologram and orthogonal circularly polarization hologram were recorded. By adjusting the Q_3 and P, the diffraction images of parallel circularly polarization hologram and of orthogonal circularly polarization hologram can be obtained individually and together, like shown in Fig.35. So it can be seen that the storage density can be doubled by using polarization multiplexing.

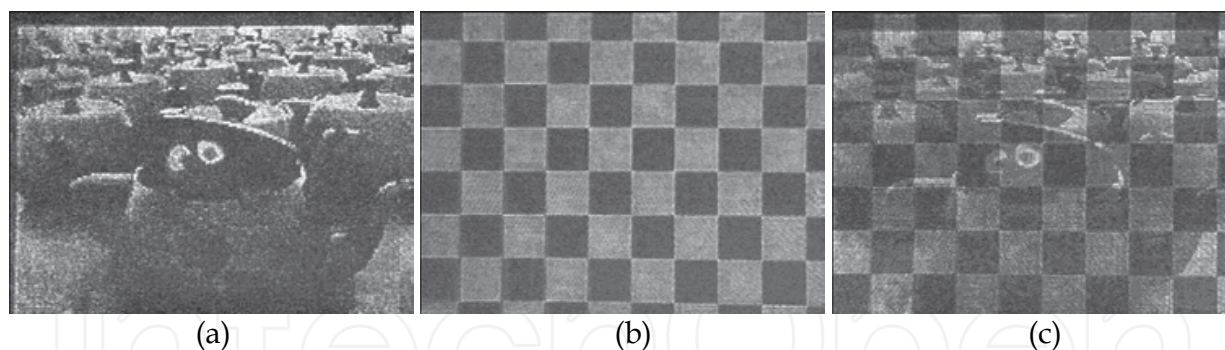| (a) | (b) | (c) |

Fig. 35. The reconstruction images in polarization multiplexing holographic storage in fulgide film: reconstruction image (a) of parallel circular polarization hologram; (b) of orthogonal circular polarization hologram; (c) of both holograms

4.7.2 Angular multiplexing holograms

Using the optical setup shown in Fig.28, the angular multiplexing holographic storage is realized. In the reference beam path, lenses L_6 and L_7 comprise a 4f system. Rotatable mirror M_2 and sample are located at the front focal plane of L_6 and at the back focal plane of L_7. When the mirror M_2 rotates within a certain range round its shaft, the exposure position of the reference beam on the sample does not move with the rotation of M_2, but only the incident angle will change, so angular multiplexing can be performed. The angle between the object wave and the normal of the sample and the angle between the centre line of

reference wave and the normal of the sample are both 45°. In the angular multiplexing, the angle between two reference beams corresponding to two neighboring holograms should be greater than the minimum horizontal selection angle $\Delta\Theta$[10] :

$$\Delta\Theta = \frac{2\sqrt{\pi^2 - v^2}\lambda}{\pi nd} \frac{\cos\theta_s}{|\sin(\theta_r - \theta_s)|} \qquad (2)$$

Where $v = \pi\Delta nd / (\lambda\sqrt{\cos\theta_r \cos\theta_s})$. In this experiment, the λ=633nm, the thickness of the sample is d=10μm, the refractive index of the sample is about n≈1.5, and for our sample at 633nm the refractive index difference between E-form and C-form is Δn≈1.7×10^{-2}, θ_r=45°, θ_s=-45°, so it can be calculated that $\Delta\Theta$≈3.16°. Because limited by the size of lens L_6 and L_7, the rotation range of M_2 is $\Delta\alpha_{max}$=8°, so the corresponding reference beam maximum multiplexing angle range is $\Delta\theta_{max}$=16°. Therefore, in this experiment, the angle between two reference beams corresponding to two neighboring holograms is chosen as $\Delta\theta$=4°. Five images were multiplexing recorded respectively with exposure time: 20s, 18s, 16s, 14s and 12s.

Reading order of diffracted images is reverse to the recording order. The read out time of each image is 0.2s. The results are shown in Fig.36. It can be seen that, no crosstalk exist between five images and the images' qualities are good. So the storage density can be increased 4 times.
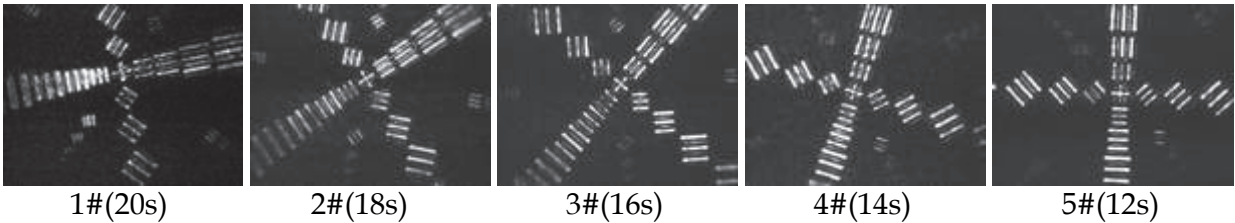

| 1#(20s) | 2#(18s) | 3#(16s) | 4#(14s) | 5#(12s) |

Fig. 36. The experimental results of angular multiplexing holograms

Because each time when a new hologram is recorded, the hologram recorded before will be erased. In multiple holograms recording, the erase to the first image is largest and the last recorded image is not affected. If each hologram is recorded for the same time, diffraction efficiency of the first hologram will be lowest, and the diffraction efficiency of final hologram will be highest. Therefore, in order to obtain same diffraction efficiency for the holograms, the exposure time should be reduced with the increasing of the recording order of holograms. The simple diagram is shown in Fig.37.
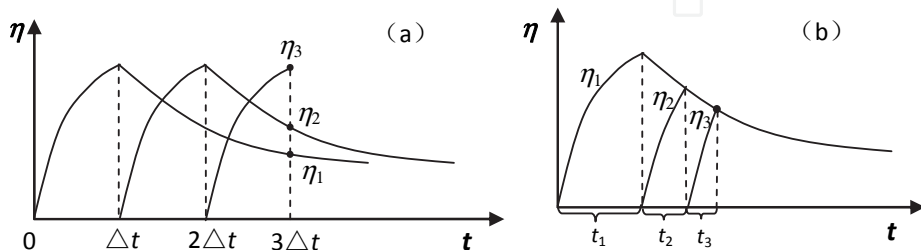

Fig. 37. A simple diagram to explain the exposure time of each hologram in holographic multiplexing: (A) condition with equivalent recording time; (b) condition with decreased recording time

4.7.3 Circumrotation multiplexing holograms

Circumrotation multiplexing is a special angular multiplexing method [10]. In basic circumrotation multiplexing light path of two recording beams unchanged. Every time when a new hologram is recorded, recording medium is rotated at an angle around an axis perpendicular to sample's surface. Fig.38a is a diagram of circumrotation multiplexing holograms, i.e. a diagram of the grating vector directions. The x-y plane is material's surface, and z axis is the rotational axis. To avoid the merger of gratings, the rotation angle of the medium must meet one of the following two conditions: (1) which is more than vertical selection angle; (2) the unnecessary reconstructed images can be filtered by the aperture of detector. The phase conjugated beam reconstruction hologram storage system shown in Fig.24 was used for the circumrotation multiplexing holograms storage experiment. According to the experimental condition, rotation angle is chosen as 10°, after 180° of rotation, 18 images are recorded at the same position of the sample. In Fig.38b, the reconstructed images of the holograms recorded at 0° and 170°are given. It can be seen that no crosstalk exist between the holograms, but reconstructed images' quality is poor.
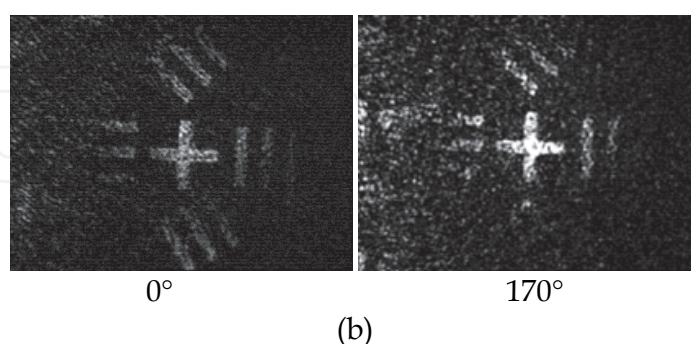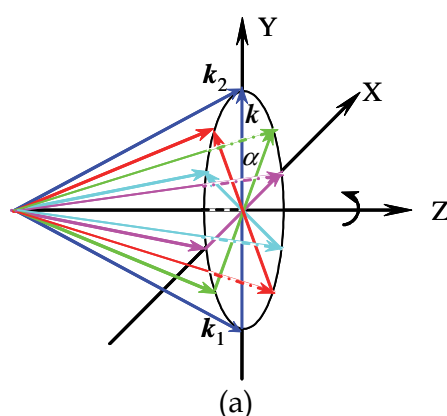

(a)

0°   170°

(b)

Fig. 38. Circumrotation multiplexing holograms storage experiment: (a) schematic diagram; (b) experimental results

4.8 Holographic interferometer based on fulgide film

Holographic interferometer is an important aspect of holographic application. At present no reports about the application of fulgide films on holographic interferometer is found. In the section, using the current experimental setups the holographic interferometer application experiment of fulgide film are carried out, including double exposure method and single exposure method.

The experimental setup shown in Fig.28 is used for holographic interferometer application experiment of fulgide film. The recording medium is placed near the frequency-plane. The process of double exposure experiment is as follows: Two holograms are recorded early or late at the same place of the sample by using same setup. When reconstructed by original reference beam, two object waves will be reconstructed together and interference with each other, whose interference fringe can be captured by the CCD. The process of real-time holographic interferometer (single exposure method) experiment is as follows: A hologram of original object beam (OB1) is recorded first. Then the object wave surface to be tested (OB2, whose intensity is decreased to similar with the diffraction light intensity) and the reference beam irradiate the hologram at the same time. The interference fringe between the diffracted wave of OB1 and transmitted wave of OB2 can be captured by the CCD.

According to the theoretical analysis and experimental results, it can be understood that the experimental results of double exposure interferometer and real-time interferometer are same, and their processing methods are same too. So here just four experimental results of double exposure interferometer are given, like shown in Fig.39.

Using data processing, the thickness variety values of measured objects at any point on the X-Y surface can be got. In Fig.40 shows the thickness variety of measured objects got by processing the experiment results shown in Fig.39(a,b). And the tilt angles of the optical wedge and of axicon are calculated as 1.83°and 1° respectively. Form Fig.39(c,d) it can be calculated that the rotation angle of optical wedge is 7.91°and the movement of axicon is 1.86 mm [11].
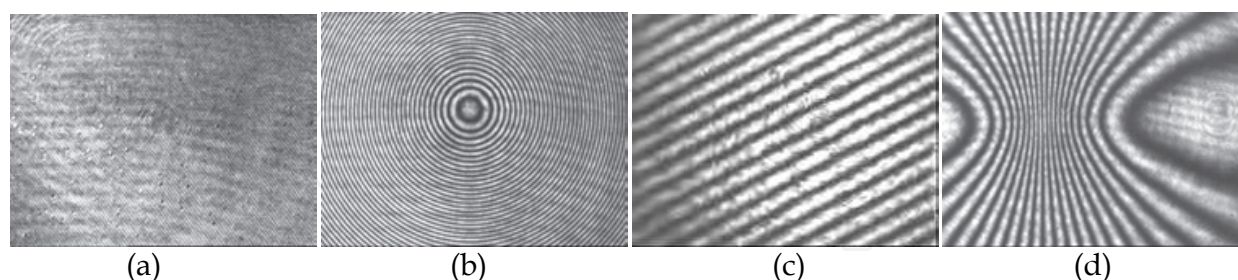

(a)   (b)   (c)   (d)

Fig. 39. Experimental results of double exposure interferometer: (a) no object(air) in the first exposure and the wedge is the object to be tested in the second exposure; (b) no object(air) in the first exposure and the axicon is the object to be tested in the second exposure; (c) the wedge is the object, which is rotated slightly in two exposure; (d) the axicon is the object, which is moved slightly toward right-or-left in two exposure
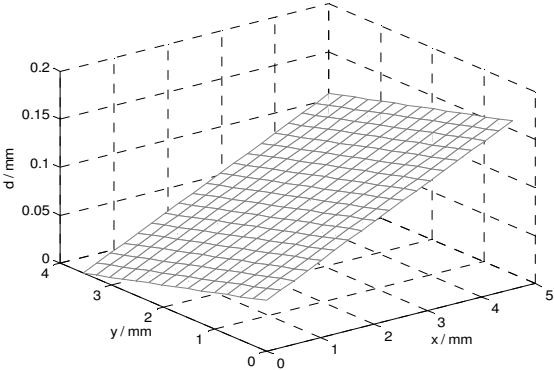
(a)
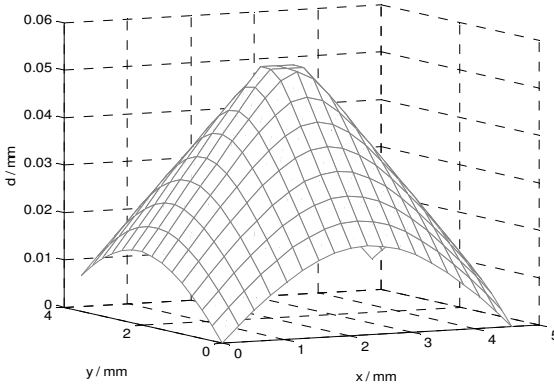
(b)

Fig. 40. (a) thick variety of optical wedge, (b) thick variety of axicon

4.8.4 Application of polarization multiplexing technique in holographic interferometer

The object to be measured is moving particle. The parallel linearly polarization hologram and orthogonal linear polarization hologram are recorded respectively, and then the two images can be reconstructed individually owing to polarization multiplexing technique, in addition the recorded order of the two holograms is known, so the direction and velocity of the object's movement can be got. But we cannot distinguish the recorded order of the two holograms if they are both recorded by parallel linearly polarization holographic technology. Fig.41 shows the experimental results (because for real moving particles the dispersion of light is too large, the transparent film is used as the measured object.)

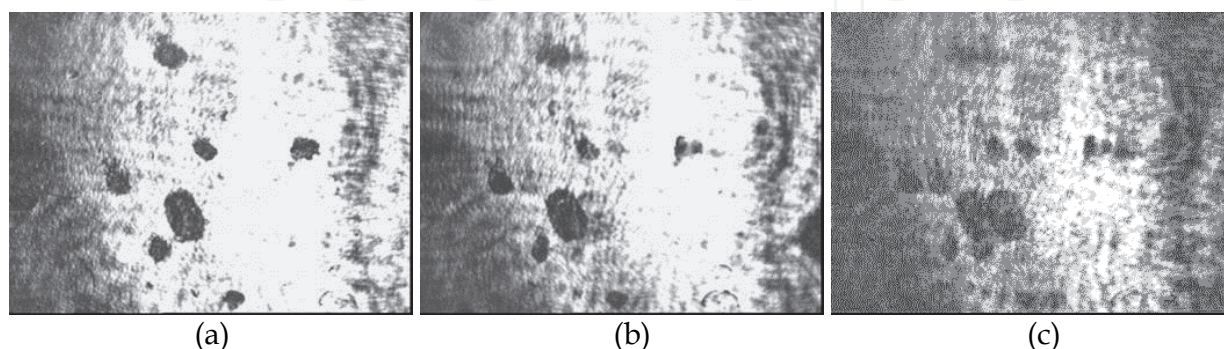| (a) | (b) | (c) |

Fig. 41. The double exposure experimental results to record movement track of the particles at different times (a) 1st image recorded as parallel linearly polarization hologram; (b) 2nd image recorded as orthogonal linearly polarization hologram; (c) reconstructed image obtained when the polarization P is rotated to 30°

5. Conclusion

The holographic storage applications of 3-indoly-benzylfulgimide/PMMA film were studied in detail including the ordinary holography and polarization holography, which are respectively based on the photochromic and photoinduced anisotropy properties. The properties of holographic recording such as diffraction efficiency, spatial resolution and optimal exposure were measured; especially the diffraction efficiency spectra and dynamic curves of different kinds of polarization holographic recording were theoretically analyzed and experimentally measured.

The holographic optical image storage was realized in the fulgide films by using different kinds of holographic storage techniques. The experimental results show that: compared with transmission-type holographic recording, reflection-type holographic recording hologram has lower diffraction efficiency and higher SNR; compared with reference beam reconstruction，the phase conjugated beam reconstruction can effectively correct the phase aberration caused by the mis-adjustment of optical setup; compared with Fraunhofer holograms, Fourier-transform holograms have lower diffraction efficiency and higher storage density; compared with parallel polarization holograms, in orthogonal polarization holograms the scattering noise can be filtered, so one can obtain high SNR, in which the orthogonal circularly polarization hologram also has high diffraction efficiency, so it is the best polarization recording method; compared with traditional non-collinear holography, the collinear holographic storage system has simpler optical setup and smaller volume,

lower environmental demand and higher storage density. The storage density of 2×10^8 bits/cm^2 was obtained in the Fourier-transform holographic data storage by using orthogonal polarization holographic recording, which had a greatly improved signal-to-noise ratio of the diffraction image.

Different kinds of multiplexing holographic storage, like polarization multiplexing, circumrotation multiplexing and angle multiplexing, were also realized in fulgide film, where 2 images, 5 images and 18 images were stored at the same position of the film, and diffracted without crosstalk with each other. And the application of the fulgide films in holographic interferometry was also studied initially.

6. References

[1] Yokoyama, Y. (2000). Fulgides for Memories and Switches. Chem. Rev., Vol.100, No.5, pp. 1717-1739

[2] Fan, M. (1997). Photon Storage Principles and Photochromic Materials. Progress in Chemistry, Vol.9, No.2, pp. 170-178 (in Chinese)

[3] Bouas-Laurent, H. & Dürr H. (2001). Organic Photochromism. Pure and Applied Chemistry. Vol.73, pp. 639–665

[4] Menke, N.; Yao, B.; Wang, Y.; Zheng, Y.; Lei, M.; Chen, G.; Chen, Y.; Fan, M. & Li, T. (2006). Optical Image Processing Using The Photoinduced Anisotropy of Pyrrylfulgide, J. Opt. Soc. Am. A, Vol.23, No.2, pp. 267-271

[5] Menke, N.; Yao, B.; Wang, Y.; Dong, W.; Lei, M.; Chen, Y.; Fan, M. & Li, T. (2008). Spectral Relationship of Photoinduced Refractive Index and Absorption Changes in Fulgide Films, Journal of Modern Optic, Vol.55, No.6, pp. 1003-1011

[6] Du, J.; Menke, N.; Yao, B.; Wang, Y. & Chen, Y. (2011). Photoreaction constants of fulgide films at different wavelengths, Proceedings of International Conference on Remote Sensing, Environment and Transportation Engineering 2011, IEEE Catalog Number: CFP1104M-PRT Volume 7, pp.6148-6154 (June 24-26, 2011, Nanjing, China)

[7] Menke, N.; Yao, B.; Wang, Y. & Chen, Y. (2011). Polarization holography in 3-indoly-benzylfulgimide/PMMA film. Journal of Atomic, Molecular, and Optical Physics Volume2011, ArticleID509507, doi:10.1155/2011/509507, pp.1-20

[8] Cheng, M.; Menke, N.; Yao, B.; Wang, Y. & Chen, Y. (2011). Improvement of the diffraction efficiency of holographic gratings in Fulgide films by auxiliary light, Proceedings of International Conference on Remote Sensing, Environment and Transportation Engineering 2011, IEEE Catalog Number: CFP1104M-PRT, Volume 7, pp.6047-6052 (June 24-26, 2011, Nanjing, China)

[9] Menke, N.; Yao, B.; Wang, Y.; Zheng, Y.; Lei, M.; Chen, G.; Chen, Y.; Fan, M.; Han, Y. & Meng, X. (2003). Holographic Recording Characteristics of a Rewritable Fulgide/PMMA Film, Acta Photonica Sinica, Vol.32, No.7, pp. 819-822 (in Chinese)

[10] Tao., S. (December 1998). Optical Holographic Storage (First Edition). Beijing University Press, Beijing, pp.267-278

[11] Ji, K.; Menke, N.; Menke, N.; Yao, B.; Wang, Y. & Chen, Y. (2011). Holographic interfermetry based on fulgide film, Proceedings of International Conference on Electronics and Optoelectroonics2011, IEEE Catalog Number: CFP1137N-PRT, Volume 3, pp.V3-276-V3-280 (July 29-31, 2011, Dalian, China)
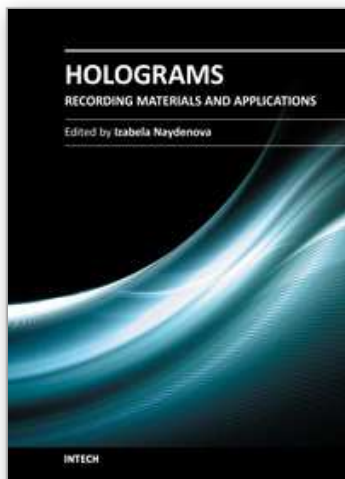
Holograms - Recording Materials and Applications

Edited by Dr Izabela Naydenova

Holograms - Recording Materials and Applications covers recent advances in the development of a broad range of holographic recording materials including ionic liquids in photopolymerisable materials, azo-dye containing materials, porous glass and polymer composites, amorphous chalcogenide films, Norland optical adhesive as holographic recording material and organic photochromic materials. In depth analysis of collinear holographic data storage and polychromatic reconstruction for volume holographic memory are included. Novel holographic devices, as well as application of holograms in security and signal processing are covered. Each chapter provides a comprehensive introduction to a specific topic, with a survey of developments to date.

How to reference

In order to correctly reference this scholarly work, feel free to copy and paste the following:

INTECH

open science | open minds